

ALICE-PUBLIC-2013-001
August 28, 2013

Charged-particle multiplicity measurement with Reconstructed Tracks in pp Collisions at $\sqrt{s} = 0.9$ and 7 TeV with ALICE at the LHC

The ALICE Collaboration*

Abstract

This note describes the details of the analysis of charged-particle pseudorapidity densities and multiplicity distributions measured by the ALICE detector in pp collisions at $\sqrt{s} = 0.9$ and 7 TeV in specific phase space regions. The primary goal of the analysis is to provide reference measurements for Monte Carlo tuning. The pseudorapidity range $|\eta| < 0.8$ is considered and a lower p_T cut is applied, at 0.15, 0.5 GeV/ c and at 1 GeV/ c . The choice of such phase space regions to measure the charged-particle multiplicity allows a direct comparison with the analogous results obtained by other LHC collaborations, namely ATLAS and CMS. The class of events considered are those having at least one charged particle in the kinematical ranges just described. In the note, the analysis procedure is presented, together with the corrections applied to the data, and the systematic uncertainty evaluation. The comparison of the results with different Monte Carlo generators is also shown.

*See Appendix A for the list of collaboration members

1 Introduction

Among the key observables in understanding the general properties of Minimum Bias proton-proton events are the pseudorapidity densities ($dN_{\text{ch}}/d\eta$) and multiplicity distributions of charged particles. The ALICE results on charged-particle pseudorapidity density and multiplicity distributions in pp collisions at $\sqrt{s} = 0.9, 2.76$ and 7 TeV were already published in [1, 2, 3]. Further measurements on the same subject, but with different event and track selection, are presented in this note for proton-proton collisions at $\sqrt{s} = 0.9$ and 7 TeV. Tracks reconstructed as coming from primary particles¹ in the Inner Tracking System (ITS) and in the Time Projection Chamber (TPC) of ALICE have been used, and a kinematical phase space defined in η ($|\eta| < 0.8$) and p_{T} ($p_{\text{T}} > p_{\text{T,cut}}$, with $p_{\text{T,cut}} = 0.5$ GeV/ c and 1.0 GeV/ c) has been considered, as agreed within the LHC Minimum Bias and Underlying Event Working Group [4]. This allows for a direct comparison between the results from the different LHC experiments (ALICE, ATLAS and CMS), while minimizing the dependence from the Monte Carlo model used for correction, and the contribution to the uncertainty coming from diffractive processes. The central pseudorapidity interval was defined according to the acceptance of the ALICE main tracking detector (the ALICE TPC). The lowest $p_{\text{T,cut}}$ value was set to 0.5 GeV/ c to comply with the ATLAS and CMS tracking efficiency. The note also includes the results in the same central rapidity interval with $p_{\text{T,cut}} = 0.15$ GeV/ c , corresponding to the $p_{\text{T,cutoff}}$ at which the ALICE global tracking efficiency (i.e. including both ITS and TPC) reaches $\sim 50\%$ and stays approximately constant ($\sim 70 - 75\%$) for higher p_{T} [5]. We measure the pseudorapidity density and multiplicity distribution of all charged particles in the mentioned kinematical region for those events which have at least one charged particle in the same kinematical region. This introduces a so-called “hadron level definition” of the event class considered, named $\text{INEL} > 0_{|\eta| < 0.8, p_{\text{T}} > p_{\text{T,cut}}}$ hereafter.

A similar analysis has already been presented in [6]. In this note, the focus is on the differences with respect to [6] and the already published results in terms of event and track selections. Section 2 will briefly describe the ALICE experiment and the data samples used for the current analysis. The analysis strategy will be discussed in Section 3. In Section 4 the systematic uncertainties taken into account will be presented. The final results will be given in Section 5. Finally, conclusions will be drawn in Section 6.

2 The ALICE experiment and the data samples

The ALICE experiment consists of a set of different detectors placed in a solenoidal magnetic field of 0.5 T (the central barrel) plus other detectors outside. Details about the various subsystems can be found in [7]. For the analysis presented herein, tracks reconstructed in the ALICE central barrel by the ITS and TPC detectors were used, while the triggering and event selection relied on both the ITS and VZERO detectors.

The Inner Tracking System (ITS) is the ALICE detector closest to the beam pipe, at a radial distance that varies between 3.9 and 43 cm. Three types of Si sensors are used for the ITS. The two innermost layers, for which a high granularity is needed to cope with the requirement to measure the position of primary and secondary vertices with high resolution, consist of Silicon Pixel Detectors (SPD), covering the pseudorapidity regions $|\eta| < 2$ and $|\eta| < 1.4$ respectively. They perform charged-particle multiplicity measurements over an extended η range. The SPD layers are followed by a pair of Silicon Drift Detectors (SDD), characterized by a very good multitrack reconstruction capability. Finally, two layers of Silicon Strip Detectors (SSD) complete the ALICE ITS. In addition to being in charge of the reconstruction of the primary and secondary vertices, the ITS contributes to the ALICE global tracking, and is as well capable to perform standalone reconstruction. This has the advantage to recover the tracks lost in the global tracking due to the limited spacial acceptance and the intrinsic $p_{\text{T,cutoff}}$ of the outer detectors, and to particle decay. Thanks to the large number of detection channels, the two SPD layers also provide

¹The ensemble of primary charged particles includes those produced in the collision and their decay products, excluding weak decays from strange particles.

ALICE with L0 trigger signals (e.g. to select Minimum Bias events or to apply multiplicity selection criteria), while dE/dx measurements are performed by SDD and SSD to identify charged hadrons at low momentum (up to ~ 1 GeV/ c and, for standalone reconstructed pions, down to ~ 100 MeV/ c).

The ALICE Time Projection Chamber (TPC), following the ITS in radial direction ($85 < r < 247$ cm), is the main ALICE tracking detector. Its pseudorapidity coverage is $|\eta| < 0.9$ for tracks with full radial track length (i.e. matching with the ITS, TRD, and TOF detectors), and $|\eta| < 1.5$ for reduced track length. The TPC tracking efficiency (defined at Monte Carlo level as the ratio between the number of tracks reconstructed by the TPC and those emitted in the TPC acceptance) reaches $\sim 80\%$ in $|\eta| < 0.8$ with a momentum resolution $\sigma(p_T)/p_T \sim 5\%$, or $\sim 2.5\%$ up to $p_T = 10$ GeV/ c (and increasing at higher transverse momenta) for combined tracking with the ITS. Each track in the TPC is reconstructed using up to a maximum of 159 space points, each measured for very high momentum tracks (i.e. with negligible curvature) with a resolution better than 0.8 mm in both the plane transverse to the beam direction (xy) and in the direction parallel to the beam (z). The TPC identifies charged hadrons in the intermediate momentum range (from ~ 0.1 up to $\sim 1 - 2$ GeV/ c) via specific energy loss measurements. Moreover, in the region of relativistic rise, where a statistical approach is utilized, the TPC can identify charged hadrons up to p_T of a few tens of GeV/ c .

The VZERO detector consists of two arrays of 32 scintillators each placed on either side of the nominal interaction vertex at a distance of 3.3 and -0.9 m and covering pseudorapidity ranges $2.8 < \eta < 5.1$ and $-3.7 < \eta < -1.7$ respectively. As already mentioned, together with the SPD, the ALICE VZERO contributes to the trigger, event selection and background rejection for this analysis.

The data samples used consisted of Minimum Bias pp events collected in 2009 and 2010. The Minimum Bias trigger was defined as a signal in either one of the two ALICE VZERO hodoscopes, or in the ITS pixel detector (one out of three). A coincidence with the signals from the two beam pick-up counters (BPTX) was also required to select the events and remove the background. In such conditions, about 110000 (collected in 2009) and 2.2×10^6 events (collected in 2010) were used for the charged-particle pseudorapidity density analysis at $\sqrt{s} = 0.9$ and 7 TeV respectively. The multiplicity distributions were obtained from approximately 2.9×10^6 and 2.7×10^6 events (all collected in 2010) at $\sqrt{s} = 0.9$ and 7 TeV respectively.

2.1 Offline event selection

In addition to requiring the Minimum Bias trigger in the collision and the reconstruction of the primary vertex, a preselection of the events aimed at reducing the beam background was applied. It relies on the ALICE VZERO timing signal and on the correlation between the number of hits and the so-called tracklets² found in the SPD detector (see also [1]). The vertex was required to be obtained either from the tracks reconstructed from the TPC and the ITS detectors, or, in case this was not available, from the tracklets, using the SPD information. Moreover, only events for which the vertex position along the z coordinate (vt_{x_z}) is such that $|vt_{x_z}| < 10$ cm were accepted. Finally, for the results presented here, only the events with at least one reconstructed track in the kinematical region defined by the pseudorapidity interval $|\eta| < 0.8$ and $p_T > p_{T,\text{cut}}$ ($p_{T,\text{cut}} = 0.15, 0.5, 1$ GeV/ c) were considered. This sample was then corrected back to the $\text{INEL} > 0_{|\eta| < 0.8, p_T > p_{T,\text{cut}}}$ “hadron level definition” mentioned in Sec. 1.

Figure 1 shows the event selection efficiencies from Monte Carlo simulations as a function of the generated charged particle multiplicity for the three $p_{T,\text{cut}}$ values at $\sqrt{s} = 0.9$ (top) and 7 TeV (bottom), obtained for the $dN_{\text{ch}}/d\eta$ analysis (after pile-up removal for the $\sqrt{s} = 7$ TeV cases, see following paragraph, and Sec. 4). As one can see, for both energies and for the three different $p_{T,\text{cut}}$ values, the efficiency is larger than $\geq 90\%$ already at a generated multiplicity of 2 particles in the range considered. The results come from the PYTHIA Monte Carlo simulations used to correct the data, with the D6T (tune 109) [8]

²A tracklet is built combining a pair of hits in the two ITS SPD layers.

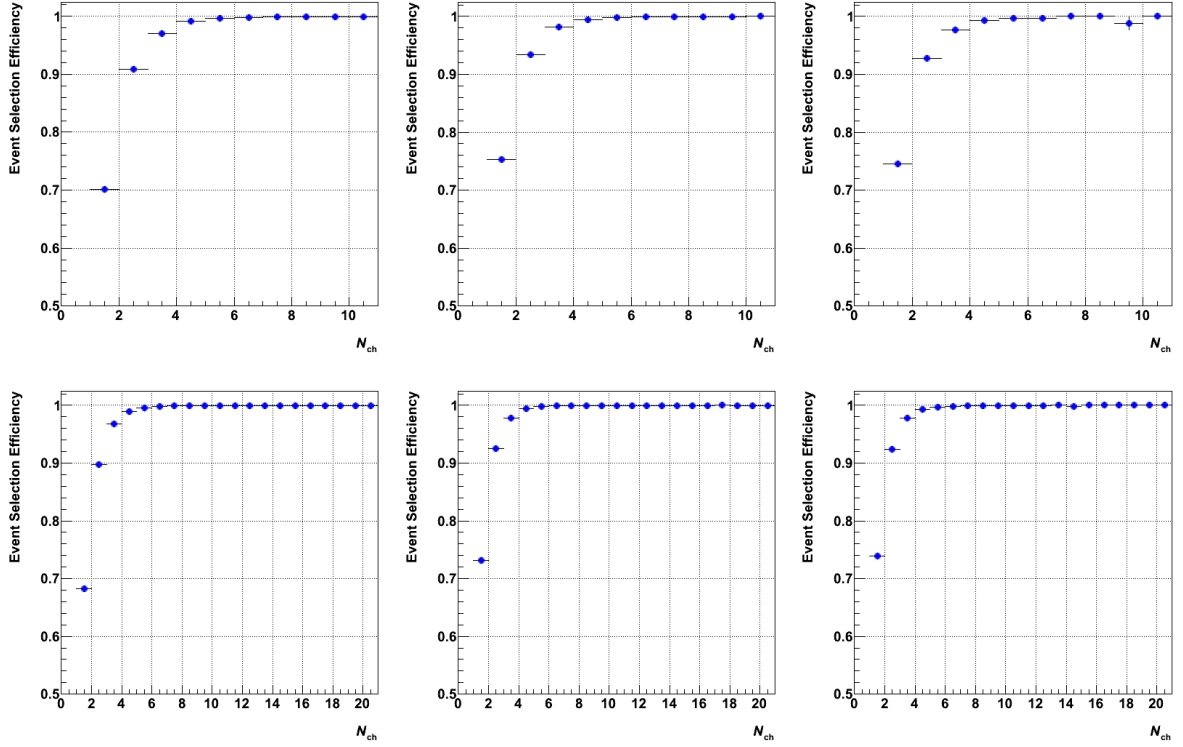


Fig. 1: Triggered event selection efficiency from Monte Carlo simulations as a function of the generated multiplicity ($|\eta| < 0.8$, $p_T > p_{T,\text{cut}}$) for pp collisions at $\sqrt{s} = 0.9$ TeV (top) and 7 TeV (bottom), for the three different values of the $p_{T,\text{cut}}$ (0.15 (left), 0.5 (middle) and 1.0 (right) GeV/c).

and Perugia-0 (tune 320) [9] tunes for the lowest and highest energy, respectively.

For the analysis of the 2010 data (for both the $dN_{\text{ch}}/d\eta$ and multiplicity distribution results), an additional criteria was included in the event selection in order to reduce the event pile-up contribution, already kept low by the specific choice of data with $\mu \lesssim 0.053^3$. Based on the SPD information, events coming from a pile-up interaction (i.e. a further collision occurring in the same bunch crossing in addition to the triggering one) were removed: vertices from pile-up collisions can be identified from tracklets not pointing to the position of the primary vertex as estimated by the tracklets themselves, provided that such secondary vertices have at least three contributors, and are separated by the primary one by at least 8 mm.

3 Analysis strategy

The tracks used in the analysis are those reconstructed by the ALICE central global tracking [10]. The tracking procedure starts with a first determination of the primary vertex through the combination of the SPD tracklets. Starting from this vertex, track seeding (i.e. the procedure to find track candidate starting from clusters) is afterwards performed in the TPC. A Kalman filter [10, 11] is then applied propagating the tracks inwards through the sensitive volume of the TPC, through ITS, building the so-called global tracks from the association of hits in the ITS to the TPC track candidates. The global tracks are then propagated outwards, to the other ALICE detectors (TPC, TRD, TOF). A last inward Kalman propagation towards the primary vertex is then performed, and the primary vertex recalculated. The full description of the method used for the primary vertex determination can be found in [10, 12].

Track selection criteria (cuts) have been applied in order to maximize the tracking efficiency and min-

³The μ coefficient corresponds to the average number of collisions per bunch crossing.

imize the contamination from secondaries and fake tracks. Besides requiring the tracks to be reconstructed by both TPC and ITS, and to reject kinks (i.e. charged kaons decaying in two particles one of which neutral), additional quality criteria are applied to optimize the reconstruction efficiency, and reduce the contamination from secondaries. These cuts include:

- the number of clusters found in the ITS (at least 1 cluster in the SPD, out of a maximum of 6, as the ITS has 2 layers per subdetector);
- the minimum number of TPC signal clusters associated to the reconstructed track (70 out of a maximum of 159);
- the χ^2 per TPC signal cluster (calculated with respect to the track parameters estimated from the track fit to an helix) used to reconstruct the momentum (at most 4);
- the distance of closest approach (dca) to the vertex in the xy plane and in the z direction (perpendicular and parallel to the beam axis, respectively).

The cut applied to the distance of closest approach in the plane perpendicular to the beam axis corresponds to a 7σ cut where σ is the resolution of the transverse impact parameter for primary tracks. Since the latter one depends on p_T , also the cut was p_T dependent (with a dependence of the form $0.035 + 0.042 \times p_T^{-0.9}$ and $0.0182 + 0.0350 \times p_T^{-1.01}$ for 2009 and 2010 data respectively). For the 2010 data, further cuts were introduced:

- on the distance of closest approach in the z direction (< 2 cm), in order to further reduce the contamination from tracks from pile-up events not rejected by the event selection;
- on the maximum value of $\chi^2/\text{ITS cluster}$ (36);
- on the maximum value for the χ^2 between the “TPC only track” constrained to the vertex and the “global track”⁴ (set to 36).

The raw $dN_{\text{ch}}/d\eta$ and multiplicity distributions obtained from data were corrected using PYTHIA Monte Carlo simulations as described in Sec. 3.1 and Sec. 3.2. The GEANT3 particle transport package was used together with a detailed description of the geometry of the experiment, and of the detector and electronics response. Moreover, the simulation was set to reproduce the conditions of the LHC beam and of the detectors (in terms of vertex position, calibration, alignment and response) at data taking for the considered data.

A comparison between the distance of closest approach in the xy plane in the data and in the PYTHIA Monte Carlo used for the corrections showed that PYTHIA underestimates the particle yield from secondaries (including the decays from strange particles), the difference varying between 0 and 35% at $\sqrt{s} = 0.9$ TeV (from D6T tune, see [5]) and between 35% and 45% at 7 TeV (from Perugia-0 tune, see also [13]), depending on p_T . To consider this, the secondaries were rescaled in the Monte Carlo to match the data. This correction was applied to all simulations used to correct the data.

3.1 Corrections for the charged-particle pseudorapidity density analysis

The charged-particle pseudorapidity distribution is given by the formula:

$$\frac{1}{N_{\text{ev}}} \frac{dN_{\text{ch}}}{d\eta} \quad (1)$$

⁴While “global tracks” are reconstructed using the full tracking information of ALICE including ITS, “TPC only track” are built considering only the TPC information.

to which three types of corrections have to be applied. First of all, a *track-to-particle* correction is needed, in order to take into account the difference between the measured tracks and the true charged primary particles. This correction takes into account acceptance effects, detector and reconstruction efficiency. It is applied at track level. Secondly, the vertex reconstruction requirement in the analysis imposes a bias on both the number of tracks and of events used, since those events without a reconstructed vertex are not considered. This bias is corrected for, at both track and event level (*vertex reconstruction* correction). Finally, the bias due to the trigger (event class) used is considered, resulting in a track level and event level *trigger bias* correction.

In the analysis, the track corrections are obtained as a function of η , the z position of the vertex (vx_z) and p_T using all reconstructed tracks fulfilling the track selection requirements. The event corrections depend on the reconstructed multiplicity and vx_z of the event and are calculated considering the events satisfying the condition of having at least one reconstructed track in the η - p_T phase space under study. For the analysis presented here, the corrections were derived from a PYTHIA Monte Carlo simulation (with the D6T [8] and Perugia-0 [9] tunes for the lower and higher energy, respectively). A complete discussion of the correction procedure can be found in [1, 6].

Table 1 summarizes the average correction factors applied at both track and event level for the analyses at $\sqrt{s} = 0.9$ and 7 TeV. The factors are reported for the three values of $p_{T,\text{cut}}$. As one can notice, there is no strong dependence on the value of $p_{T,\text{cut}}$, even though the event level corrections slightly increase from the lowest to the highest cut.

\sqrt{s} (TeV)	0.9			7		
$p_{T,\text{cut}}$ (GeV/c)	0.15	0.5	1.0	0.15	0.5	1.0
Track level	1.389	1.301	1.317	1.455	1.362	1.361
Event level	1.071	1.122	1.204	1.070	1.1	1.142

Table 1: Average track and event correction factors in the $dN_{\text{ch}}/d\eta$ analysis at $\sqrt{s} = 0.9$ and 7 TeV.

3.2 Corrections for multiplicity distribution analysis

For the multiplicity analysis, two different corrections have to be considered.

The first takes into account the efficiency, acceptance and detector effects that result in a multiplicity spectrum distorted from the true one. In order to recover the true spectrum, an unfolding procedure was applied, building a response matrix from a Monte Carlo simulation, characterized by a high multiplicity reach, as required by the unfolding. This was possible since the measured spectrum coming from a specific true multiplicity depends only on the reconstruction procedure and the detector behaviour and not on the Monte Carlo model.

The second correction for vertex reconstruction and event selection efficiency was evaluated using a different Monte Carlo simulation, the aim of which was primarily to reproduce the multiplicity distribution of the data as closely as possible, without interfering with the relative contributions of the different processes included in the generator. The corrections were obtained from PYTHIA simulations using the ATLAS CSC [14] and Perugia-0 [9] tunes for the response matrix and event selection efficiency respectively.

The unfolded spectrum was obtained using a χ^2 -minimization procedure. The χ^2 function used to evaluate the “guessed” unfolded spectrum U , can be written as:

$$\hat{\chi}^2(U) = \sum_m \left(\frac{M_m - \sum_t R_{mt} U_t}{e_m} \right)^2 \quad (2)$$

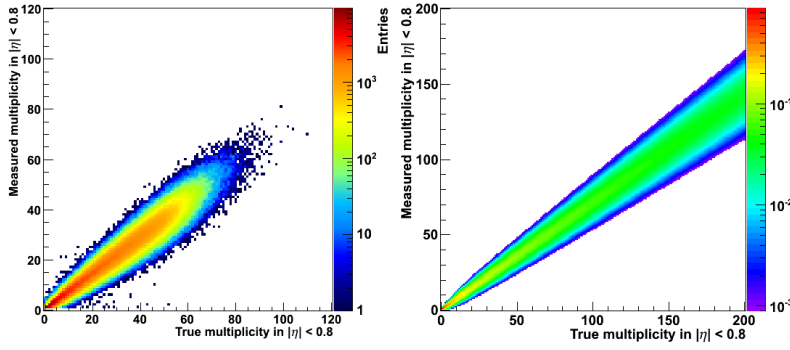


Fig. 2: Response matrices for the analysis at $\sqrt{s} = 7$ TeV for $p_{T,\text{cut}} = 0.15$ GeV/c. The left panel shows the response matrix as from the Monte Carlo simulation, while the right panel shows the parameterized response described in the text.

where M_m is the measured distribution at true multiplicity t with error e_m , and R_{mt} is the response matrix element for measured multiplicity m and true multiplicity t . As the result of this minimization suffers from oscillations in the unfolded spectrum, a constraint $P(U)$ was added to the χ^2 function, favoring a certain shape in the unfolded distribution [15]. The constraint $P(U)$ is called *regularization term*, and the new χ^2 function becomes:

$$\chi^2(U) = \hat{\chi}^2(U) + \beta P(U)$$

As written in the formula, $P(U)$ depends only on the unfolded spectrum U . β is the weight of the regularization term. Different functions can be used for the regularization term. For the results presented herein, two regularizations were considered, also to evaluate the systematic effect coming from the choice of the regularization itself. In particular, the regularizations

$$P_1(U) = \sum_t \frac{(U'_t)^2}{U_t} = \sum_t \frac{(U_t - U_{t-1})^2}{U_t} \quad (3)$$

and

$$P_2(U) = \sum_t \frac{(U''_t)^2}{U_t} = \sum_t \frac{(U_{t-1} - 2U_t + U_{t+1})^2}{U_t} \quad (4)$$

were used. The first regularization imposes constant relative "fluctuations" on the unfolded spectrum, while the second one favors the minimal relative curvature. The weight of the regularization was damped during the unfolding to account for the fact that the shape of the measured distribution might be different from the one imposed by the regularization itself, especially at low multiplicity where a typical shoulder is expected. Such damping factor was function of the measured spectrum.

An exhaustive description of the unfolding procedure can be found in [2, 6].

In order to take into account the fact that the response matrices may suffer from lack of statistics at high multiplicities and in the tails of the distributions for a given fixed true multiplicity, a parameterization of the response matrices was calculated (reproducing the Monte Carlo generated one) and used in this analysis for the unfolding of the measured data at high multiplicities. The parameterization was based on a Gaussian fit of the measured multiplicity distribution for each true multiplicity value. The mean and sigma fit values were in turn fitted with a linear function and a Padé approximation respectively. The left panel of Figure 2 shows as an example the response matrix for the analysis at $\sqrt{s} = 7$ TeV, $p_{T,\text{cut}} = 0.15$ GeV/c. The result from the parameterization is illustrated in the right panel of the same figure.

The quality of the regularization can be estimated considering the normalized residuals, defined as:

$$r_i = \frac{M_i - R \otimes U}{e_i}$$

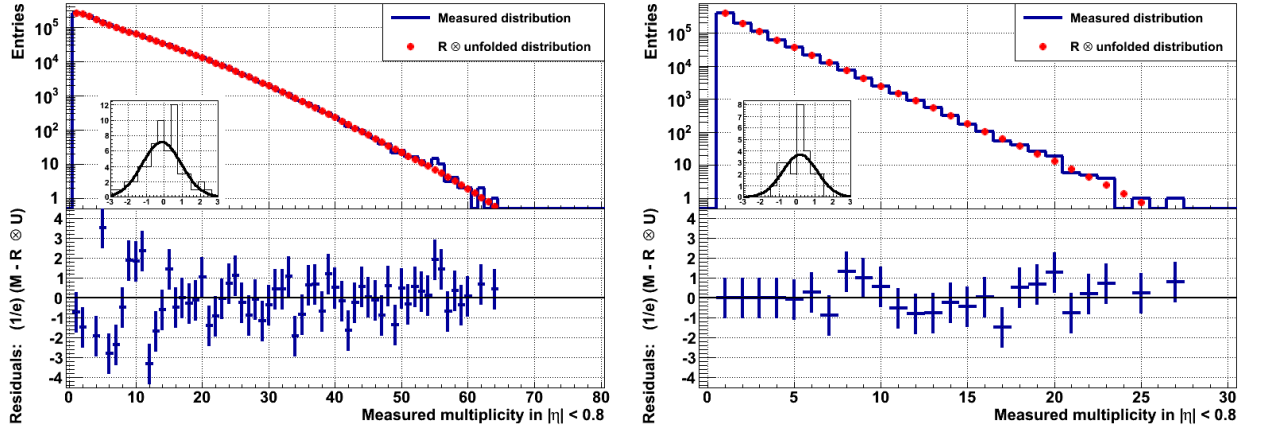


Fig. 3: Comparison between the measured multiplicities and the convolution between the response matrix and the unfolded distribution for 7 TeV data. The lower parts of the plots show the corresponding residuals as a function of multiplicity. The insets represent the residual distributions, with the Gaussian fit superimposed. The two $p_{T,\text{cut}}$ values 0.15 (left), and 1.0 (right) GeV/ c are presented.

\sqrt{s} (TeV)	0.9			7		
$p_{T,\text{cut}}$ (GeV/ c)	0.15	0.5	1.0	0.15	0.5	1.0
MC Generator	-1.8%	-1.2%	+0.6%	-2.9%	-1.1%	+1.7%
Track Selection Cuts	1.5%	0.9%	0.8%	2.0%	2.0%	1.2%
Material Budget	0.5%	0.3%	0.2%	0.5%	0.3%	0.2%
Particle Composition	1.0%	0.8%	0.5%	0.8%	0.6%	0.4%
Diffraction	0.4%	0.3%	negl.	1.0%	0.6%	negl.
ITS Efficiency	0.3%	negl.	negl.	1.0%	1.0%	1.0%
TPC Efficiency	1.5%	0.6%	0.4%	1.16%	negl.	negl.
Secondary Particle Rejection	0.8%	0.5%	0.5%	2.0%	1.5%	1.0%
Detector Misalignment	negl.	negl.	negl.	negl.	negl.	negl.
Beam-gas Events	negl.	negl.	negl.	negl.	negl.	negl.
Pile-up Event	negl.	negl.	negl.	0.4%	0.4%	0.4%
Total	+2.6% -3.1%	+1.5% -1.9%	+1.3% -1.2%	+3.5% -4.6%	+2.9% -3.1%	+2.6% -1.9%

Table 2: Contributions to the systematic uncertainty in the measurement of $dN_{\text{ch}}/d\eta$ at $\sqrt{s} = 0.9$ and 7 TeV as a function of $p_{T,\text{cut}}$. In the pseudorapidity range considered, the uncertainties showed to be $|\eta|$ independent. For this reason, one value only is reported (for $\eta = 0$).

where $R \otimes U$ is the convolution of the response matrix with the unfolded spectrum, and e_i is the error on the measured multiplicity. In the case of a satisfactory unfolding, the sum of the normalized residuals should be close to the number of degrees of freedom, i.e. the number of multiplicity bins considered. This translates in a residuals' distribution following the shape of a Gaussian function centered around zero and approximately one unit wide. Figure 3 shows the distribution of the residuals for the analysis at $\sqrt{s} = 7$ TeV, for two $p_{T,\text{cut}}$ example cases, 0.15 and 1.0 GeV/ c .

As already stated, a second correction was applied to the unfolded distribution, in order to take into account the event selection efficiency. This correction was also obtained from a PYTHIA Monte Carlo simulation, and is reported in Figure 4. As one can see, such efficiency is different from 1 only at low multiplicities ($\lesssim 5$) as expected from the definition of the events used in the analysis.

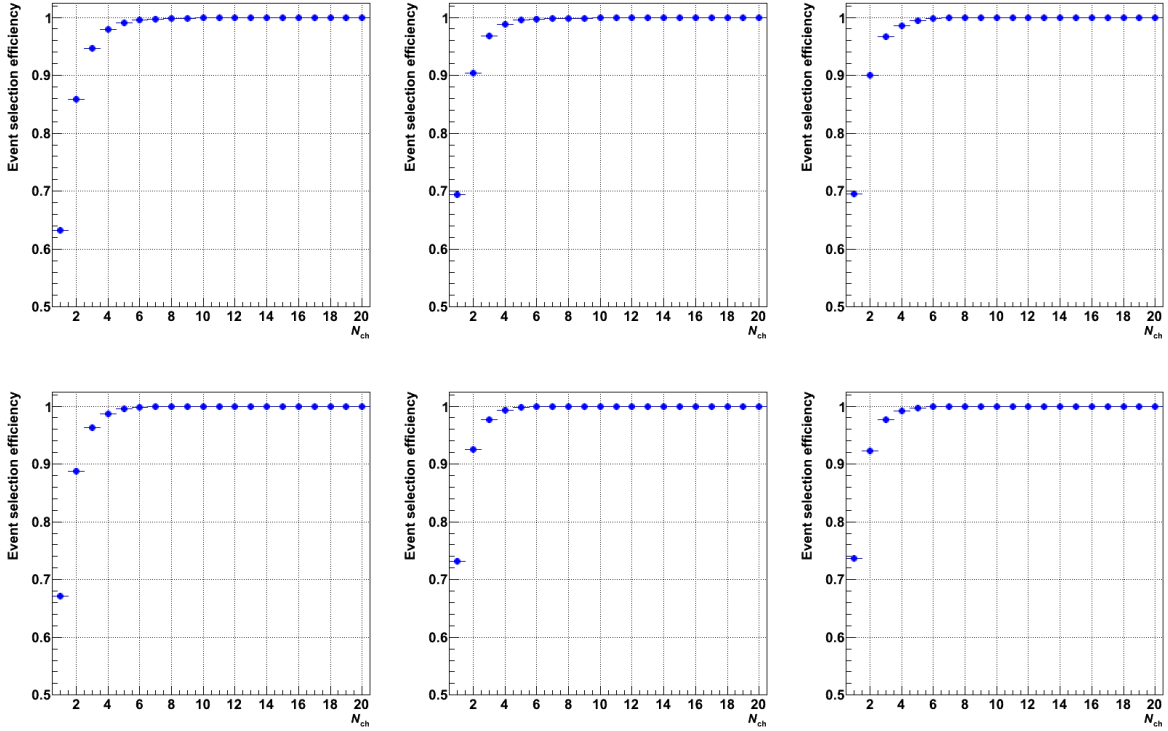


Fig. 4: Event selection efficiency from Monte Carlo simulations used in the multiplicity analysis as a function of multiplicity ($|\eta| < 0.8$, $p_T > p_{T,\text{cut}}$) for pp collisions at $\sqrt{s} = 0.9$ TeV (top) and 7 TeV (bottom), for the three different values of the $p_{T,\text{cut}}$ (0.15 (left), 0.5 (middle) and 1.0 (right) GeV/ c).

4 Systematic uncertainties

Various sources of systematic uncertainties have been taken into account in the analysis, most of which are common to the two analyses, as listed below:

- track quality cuts variation, including secondary particle rejection; this error accounts for the non-perfect agreement between the distributions of the cut variables in data and Monte Carlo;
- difference between data and Monte Carlo in terms of ITS and TPC tracking efficiency (respectively, prolongation efficiency from TPC to ITS, and efficiency in the propagation to the TPC entrance of the ITS standalone tracks; this contribution was evaluated rescaling the Monte Carlo tracking efficiency by the difference with the one found in data;
- material budget uncertainty, affecting the Monte Carlo simulations; this effect was taken into account rescaling the tracking efficiency in Monte Carlo by the effect of the change by $\pm 7\%$ in the material budget;
- relative composition of particle species which may be different in data and Monte Carlo; this was evaluated varying in the Monte Carlo simulation the relative contributions of the produced particle types by $\pm 30\%$ with respect to the values found in the generators;
- relative fraction of Single-Diffractive (SD), Non-Diffractive (ND), Double-Diffractive (DD) processes which may be different in data and Monte Carlo; this systematic error was obtained by rescaling the relative contributions of the different process types found in Monte Carlo by:

\sqrt{s} (TeV)	0.9		
$p_{T,\text{cut}}$ (GeV/c)	0.15 (5-25-35)	0.5 (5-12-22)	1.0 (4-8-14)
MC Generator	0.1 – 0.1 – 1.2%	0.2 – 0.2 – 0.2%	0.3 – 0.2 – 0.2%
Track Selection Cuts	0.6 – 2.8 – 9.1%	2.0 – 7.4 – 15.5%	4.3 – 5.3 – 17.7%
Material Budget	0.3 – 3.4 – 5.4%	1.4 – 2.2 – 3.9%	1.0 – 1.6 – 1.8%
Particle Composition	0.7 – 2.0 – 3.1%	3.6 – 2.5 – 2.9%	4.8 – 5.7 – 7.3%
Diffraction	0.4 – 0.1 – negl.%	0.1 – 0.1 – 0.1%	0.1 – 0.1 – 0.3%
ITS Efficiency	0.1 – 1.0 – 1.6%	negl.	negl.
TPC Efficiency	0.6 – 9.8 – 15.5%	2.6 – 4.6 – 8.1%	1.9 – 3.2 – 3.6%
Detector Misalignment	negl.	negl.	negl.
Beam-gas Events	negl.	negl.	negl.
Pile-up Event	0.1 – 0.3 – 1.1%	0.6 – 1.1 – 0.5%	0.7 – 1.5 – 0.6%
Unfolding	2.1 – 0.4 – 0.5%	0.1 – 6.0 – 14.4%	7.4 – 1.8 – 27.5%
Bias	5.9 – negl. – negl. %	negl. – 10.6 – negl.%	3.8 – 19.9 – negl.%
Total	6.4 – 11.0 – 19.2%	5.1 – 15.4 – 23.2%	10.8 – 21.8 – 33.8%

Table 3: Contributions to the systematic uncertainty in the measurement of the multiplicity distribution at $\sqrt{s} = 0.9$ TeV. Due to the variation of the effect along the multiplicity spectrum, three reference multiplicities are quoted for each component (low-intermediate-high). Here, the secondary particle rejection error is included in the contribution named “Track Selection Cuts”.

- $dN_{\text{ch}}/d\eta$ analysis: the measured values from U5 were used for the results at $\sqrt{s} = 0.9$ TeV (see also [1]); since no measurements were available for the 7 TeV case, the ratios from the Monte Carlo generator were used and varied by $\pm 50\%$ (see also [2]);
- multiplicity analysis: the values published in [16] (not available at the time of the $dN_{\text{ch}}/d\eta$ analysis) were used;
- pile-up rejection (for 2010 data only); such uncertainty was estimated comparing the results with and without pile-up rejection;
- Monte Carlo generator dependence, comparing the results when PHOJET⁵ [17] was used to calculate the corrections.

The effect of detector misalignment and contamination from beam-gas events was found to be negligible for both analyses.

For the multiplicity distribution analysis, two further contributions have been taken into account. Namely:

- uncertainty coming from the choice of the regularization (both function type and weight);
- bias introduced by the regularization (see [18])⁶.

The difference between data and Monte Carlo in the $\langle p_T \rangle$ distribution as a function on multiplicity was also studied. It was found that such difference, which depends on the Monte Carlo generator, has an effect on the response matrix where the correlation between the $\langle p_T \rangle$ and the multiplicity plays a role due to the p_T dependence of the tracking efficiency. The effect on the unfolded spectrum is not negligible for the multiplicity analysis at 7 TeV, especially in the high multiplicity range. To take this into account,

⁵Such uncertainty was considered asymmetric only for the $dN_{\text{ch}}/d\eta$ analysis, and symmetric for the multiplicity results, due to the variation along the multiplicity spectrum that it shows.

⁶The systematic uncertainty coming from the bias due to the regularization was added in quadrature to the final systematic uncertainty only in case it was larger than the statistical uncertainty.

\sqrt{s} (TeV)	7		
$p_{T,\text{cut}}$ (GeV/c)	0.15 (5-35-70)	0.5 (5-15-35)	1.0 (5-12-22)
MC Generator	0.1 – 0.1 – 0.2%	0.1 – 0.1 – 0.1 – %	0.4 – 0.5 – 0.5%
Track Selection Cuts	0.5 – 3.1 – 5.9%	0.4 – 1.7 – 3.2%	0.5 – 5.8 – 10.1%
Material Budget	0.2 – 2.3 – 6.8%	0.2 – 1.0 – 3.1%	0.3 – 1.1 – 2.0%
Particle Composition	0.3 – 2.2 – 7.8%	0.6 – 0.8 – 2.4%	2.4 – 3.8 – 4.7%
Diffraction	0.2 – 0.2 – 3.9%	0.2 – 0.1% – negl.	0.2 – 0.1 – 0.1%
ITS Efficiency	0.5 – 3.9 – 9.9%	0.7 – 2.5 – 7.5%	1.3 – 4.4 – 3.2%
TPC Efficiency	0.5 – 5.2 – 14.9%	0.1 – 0.3 – 0.9%	negl.
Detector Misalignment	negl.	negl.	negl.
Beam-gas Events	negl.	negl.	negl.
Pile-up Event	0.4 – 1.4 – 0.7%	0.4 – 1.3 – 3.2%	negl. – 3.1 – 15.5%
Unfolding	1.0 – 2.3 – 3.6%	0.4 – 1.4 – 3.5%	3.8 – 2.3 – 4.4%
Bias	negl. – 4.0 – negl.%	negl. – negl. – negl.	negl. – negl. – negl.
Response Matrix	0.4 – 4.1 – 10.3.%	0.4 – 0.6 – 2.8%	1.3 – 0.3 – 9.1%
Total	1.5 – 10.1 – 24.4%	1.3 – 3.8 – 10.6%	4.9 – 9.2 – 22.0%

Table 4: Contributions to the systematic uncertainty in the measurement of the multiplicity distribution at $\sqrt{s} = 7$ TeV. Due to the variation of the effect along the multiplicity spectrum, three reference multiplicities are quoted for each component (low-intermediate-high). Here, the secondary particle rejection error is included in the contribution named “Track Selection Cuts”.

at $\sqrt{s} = 7$ TeV, the average of the corrected spectra obtained from the response matrix from two different PYTHIA-6 tunes (namely ATLAS CSC [14] and Perugia-0 [9]) was used. The choice of these tunes was justified by the fact that their $\langle p_T \rangle$ vs multiplicity dependence underestimates and overestimates, respectively, the one found in data (see also [5]).

Table 2 summarizes the contributions to the total systematic uncertainty of the different sources, estimated for $\sqrt{s} = 0.9$ TeV and 7 TeV, with the three values of the $p_{T,\text{cut}}$ for the $dN_{\text{ch}}/d\eta$ results. For the multiplicity analysis, the systematic uncertainties vary as a function of multiplicity. For this reason, to give an indication of their magnitude, Tables 3 and 4 report the errors associated to only three multiplicity bins, chosen so to lie in the low, intermediate, and high multiplicity region of the unfolded spectrum, to be used as examples. To ensure a monotonic increasing behaviour of the systematic uncertainty for the multiplicity analysis, a smoothing procedure was applied for the final results suppressing the fluctuations between bins due mainly to unfolding effects.

5 Results

5.1 $dN_{\text{ch}}/d\eta$ results

Figures 5, 6, 7 show the final charged particle $dN_{\text{ch}}/d\eta$ for the two energies $\sqrt{s} = 0.9$ (left panels) and 7 TeV (right), and the three $p_{T,\text{cut}}$ values 0.15, 0.5, and 1.0 GeV/c, for the $\text{INEL} > 0_{|\eta| < 0.8, p_T > p_{T,\text{cut}}}$ classes of events. Predictions from Monte Carlo generators are superimposed on the distributions. They are indicated as follows:

- PYTHIA-6
 - Atlas CSC (tune 306 [14]);
 - D6T (tune 109 [8]);
 - A (tune 100 [19]);

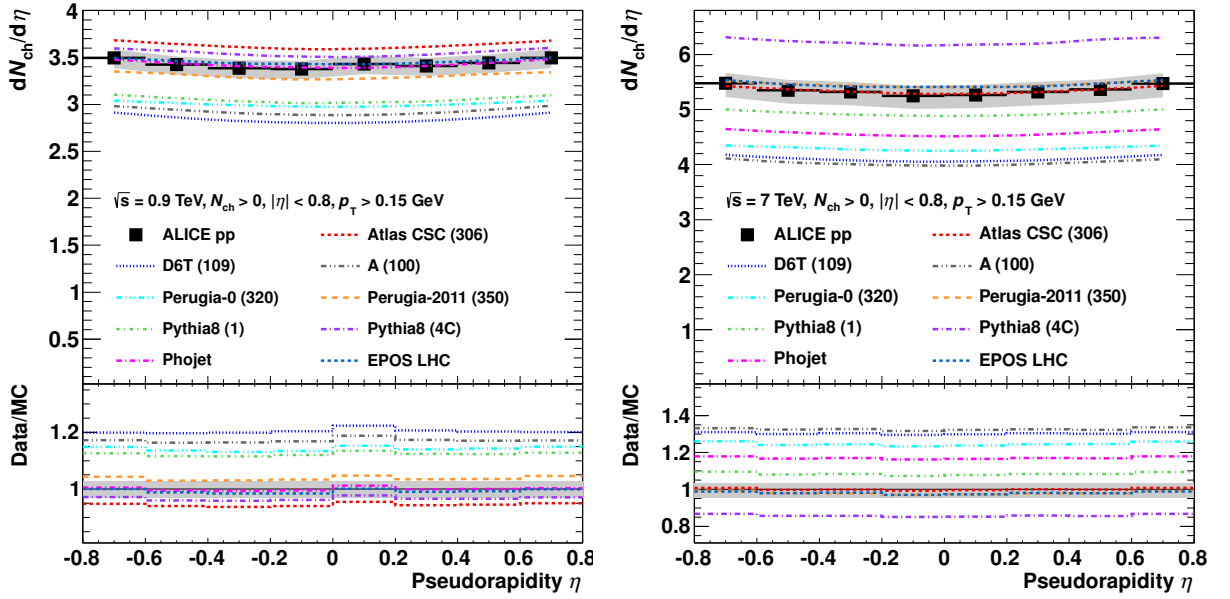


Fig. 5: Top panels: $dN_{\text{ch}}/d\eta$ versus η obtained at $\sqrt{s} = 0.9$ (left) and 7 TeV (right) with $p_{\text{T}} > 0.15$ GeV/ c for $|\eta| < 0.8$ normalized to the $\text{INEL} > 0_{|\eta| < 0.8, p_{\text{T}} > p_{\text{T, cut}}}$ event class. The predictions from different Monte Carlo generators are also shown. The grey bands represent the systematic uncertainties on the data. Bottom panels: data over Monte Carlo prediction ratios for the different generators considered. Here, the grey bands represent the total (statistical + systematic) uncertainty on the data.

- Perugia-0 (tune 320 [9]);
- Perugia-2011 (tune 350 [20]).
- PYTHIA-8
 - Pythia8 (tune 1 [21]);
 - Pythia8 (tune 4C) [22]);
- PHOJET ([17]);
- EPOS LHC ([23]).

The bottom panels of the figures show the ratio between the data and the Monte Carlo predictions. As one can see, the EPOS Monte Carlo is able to well describe the ALICE results at both centre-of-mass energies and for the three $p_{\text{T, cut}}$ values, with the largest discrepancy of $\sim 5\%$ for $\sqrt{s} = 0.9$ TeV and $p_{\text{T, cut}} = 1$ GeV/ c . For the rest of the generators, at different centre-of-mass energies and with different values of the $p_{\text{T, cut}}$, the different models describe the data differently, with a discrepancy between data and Monte Carlo that varies between a few percents and $\sim 40\%$. In general, with the exception of EPOS, a universal trend can not be identified, and the Monte Carlo prediction that agrees with the data may be different from case to case. For example, at both $\sqrt{s} = 0.9$ and 7 TeV, the ATLAS CSC tune comes quite close (within $\sim 5\%$) to the data for $p_{\text{T, cut}} = 0.15$ and 0.5 GeV/ c , even if it is not always the best prediction (e.g., at 0.9 TeV, $p_{\text{T, cut}} = 0.15$ GeV/ c the PHOJET and EPOS results are the most similar to the ALICE measured ones). On the contrary, in the case of $p_{\text{T, cut}} = 1$ GeV/ c , the difference with data is considerable ($\sim 10 - 20\%$). At $p_{\text{T, cut}} = 1.0$ GeV/ c , Perugia-0 and PYTHIA8 (tune 1) are the Monte Carlo that have the smallest discrepancy (within a few percent) to data at $\sqrt{s} = 0.9$ and 7 TeV respectively (excluding EPOS).

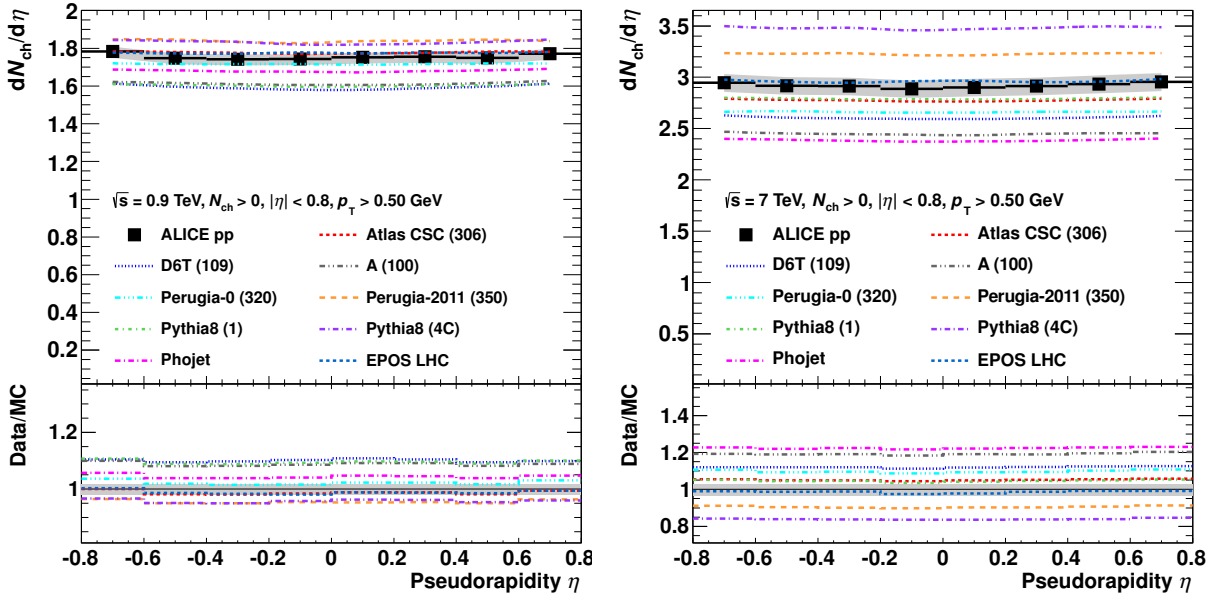


Fig. 6: Same as Figure 5, but for $p_T > 0.5$ GeV/ c .

The corresponding ATLAS results (for the two highest $p_{T,\text{cut}}$ values only) can be found in [24], where analogous conclusions were drawn.

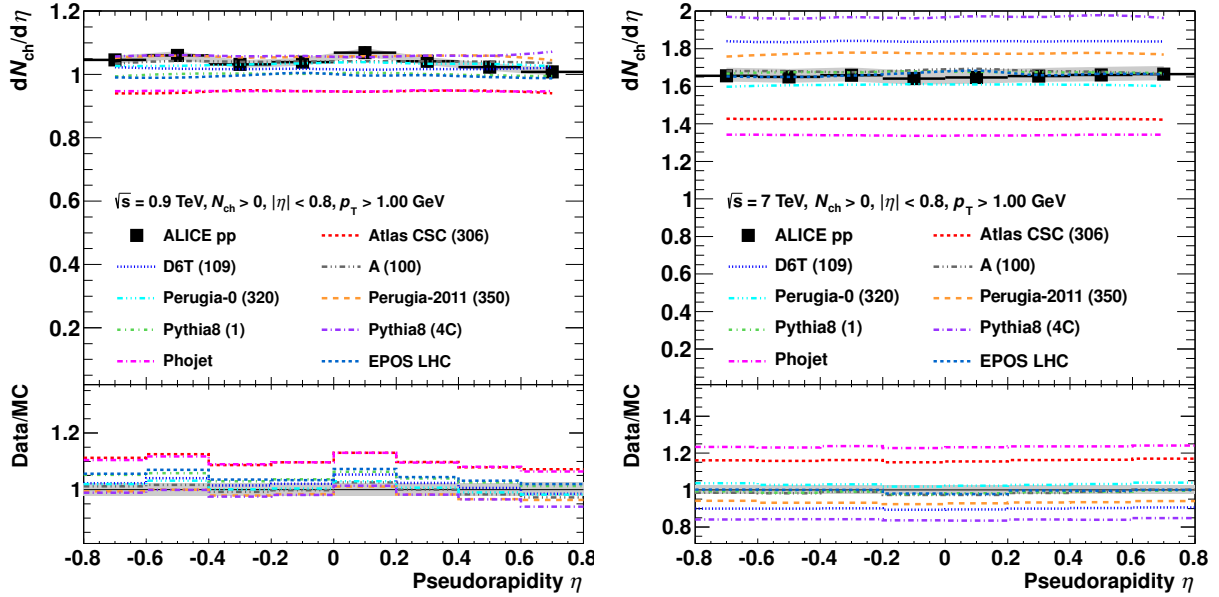


Fig. 7: Same as Figure 5, but for $p_T > 1.0$ GeV/ c .

5.2 Multiplicity distribution results

The charged particle multiplicity distribution results are illustrated in Figs. 8, 9, and 10, for the two energies $\sqrt{s} = 0.9$ (left panels) and 7 TeV (right panels), and the three $p_{T,\text{cut}}$ values 0.15, 0.5, and 1.0 GeV/ c , for the $\text{INEL} > 0_{|\eta| < 0.8, p_T > p_{T,\text{cut}}}$ classes of events. The statistical uncertainties (which are drawn separately from the systematical ones) present a non-monotonic behaviour, which is a consequence of

the usage of the specific regularization with damping in the unfolding procedure as discussed in Sec. 3.2. As one can observe, going from the lowest to the highest value of $p_{T,\text{cut}}$ for both centre-of-mass energies, the shape of the distribution becomes more exponential, with the typical shoulder at low multiplicities progressively suppressed.

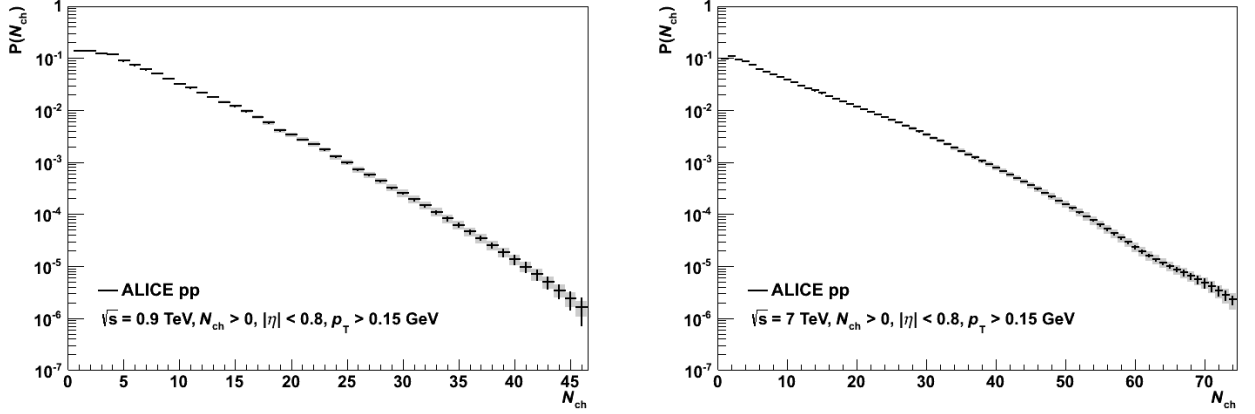


Fig. 8: Multiplicity distributions measured by ALICE at $\sqrt{s} = 0.9$ (left) and 7 TeV (right) for $p_T > 0.15$ GeV/ c . The grey bands represent the systematic uncertainty on the measurement.

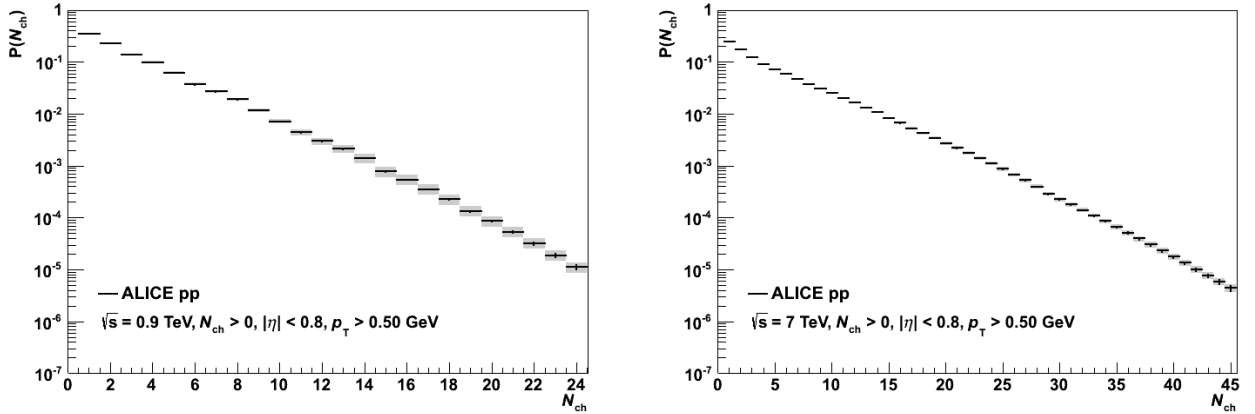


Fig. 9: Same as Figure 8, but for $p_T > 0.50$ GeV/ c .

For the sake of clarity, the comparison to the Monte Carlo calculations is reported in Figs. 11 and 12 as follows:

- Figure 11:
 - PYTHIA-6, Atlas CSC (tune 306 [14]);
 - PYTHIA-6, D6T (tune 109 [8]);
 - PYTHIA-6, A (tune 100 [19]);
 - PYTHIA-6, Perugia-0 (tune 320 [9]);
 - PYTHIA-8, 1 (tune 1 [21]);
- Figure 12:

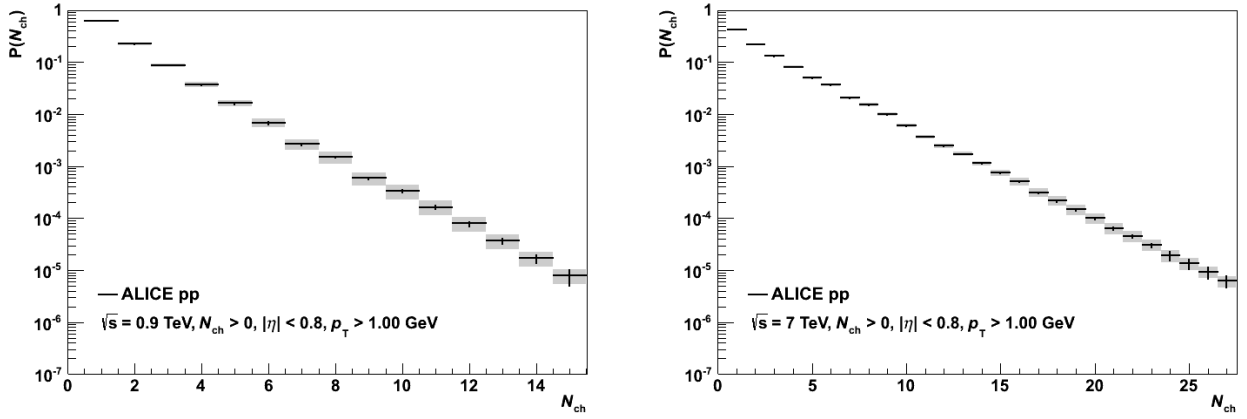


Fig. 10: Same as Figure 8, but for $p_T > 1.0$ GeV/ c .

- PYTHIA-6, Perugia-2011 (tune 350 [20]);
- PYTHIA-8, 4C (tune 4C, [22]);
- PHOJET ([17]);
- EPOS LHC ([23]).

The comparison is presented in a limited range of multiplicity in order to take into account the limited statistics available in the Monte Carlo simulations. In particular, the spectrum is shown whenever the statistical error on the Monte Carlo calculation is smaller than 10%. Moreover, a rebinning in the high multiplicity range was applied to compare to data in Figs. 8, 9 and 10 .

As it was already pointed out for the pseudorapidity density distribution results in Sec. 5.1, at different centre-of-mass energies and with different values of $p_{T,\text{cut}}$, the different models describe the data differently, and no general agreement can be observed. The level of agreement/disagreement varies significantly as a function of multiplicity, and one tune that gives reasonable comparison to data in one case (i.e. ATLAS CSC for the 7 TeV case, $p_{T,\text{cut}} = 0.5$ GeV/ c up to multiplicity $\sim 20 - 25$) fails in the others. EPOS is an exception: at both $\sqrt{s} = 0.9$ and 7 TeV it reproduces the measured distributions quite well, especially for the two lowest $p_{T,\text{cut}}$ values. PYTHIA-8 is an interesting case. The tune 1 seems to be able to reproduce within 20% the data at 7 TeV for all three values of $p_{T,\text{cut}}$, but only up to intermediate multiplicities (e.g. up to ~ 20 for $p_{T,\text{cut}} = 0.15$ GeV/ c). Nevertheless it stays far from the data at 0.9 TeV in the two lowest $p_{T,\text{cut}}$ cases. On the contrary, PYTHIA-8 tune 4C is far from the ALICE measurements at 7 TeV, especially in the high multiplicity range where it overestimates the data by up to $\sim 50\%$, but it is close to those at 0.9 TeV (within $\sim 20\%$). These considerations lead to infer that the various Monte Carlo tunes are very sensitive to the energy and general properties of the system, such as its p_T spectrum.

Similar results and conclusions for both energies and $p_{T,\text{cut}} = 0.5$ and 1.0 GeV/ c were obtained by the ATLAS experiment [24].

It is worth to mention that the comparison of the multiplicity distributions with PYTHIA-8 (tune 1, from [25]) showed by CMS in [26] suggests a good agreement between the model and the data. However, the track and event selection there ($p_T > 0$ and $|\eta| < 2.4$, Non-Single-Diffractive (NSD) events in [26]) are different from those used for the analysis presented here.

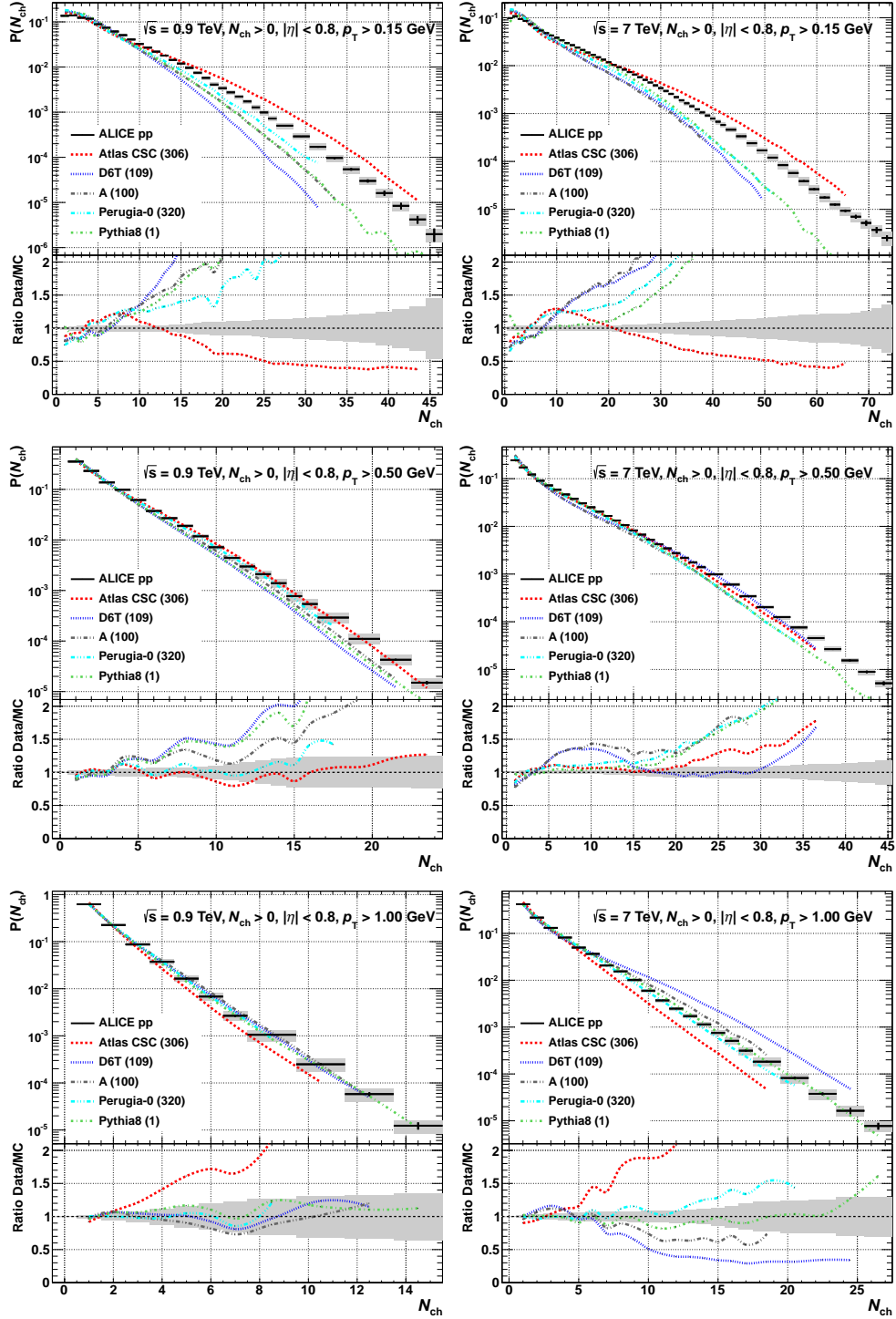


Fig. 11: Comparison with Monte Carlo predictions for the analysis at $\sqrt{s} = 0.9$ (left) and 7 TeV (right). The PYTHIA-6 tunes ATLAS-CSC, D6T, A, and Perugia-0 are drawn, together with tune 1 from PYTHIA-8 (see text for references). The $p_{T,\text{cut}}$ is 0.15, 0.5, 1.0 GeV/c from top to bottom. In the upper panels, data are showed with both the statistical (black line) and systematic (grey band) uncertainties. The grey bands in the lower panels, where the ratios data/Monte Carlo are presented, correspond the total uncertainty on the final results. The wiggles in the ratios are due to interpolations between the points at various multiplicities. The Monte Carlo calculations are showed only in the range where their statistical uncertainty did not exceed 10%.

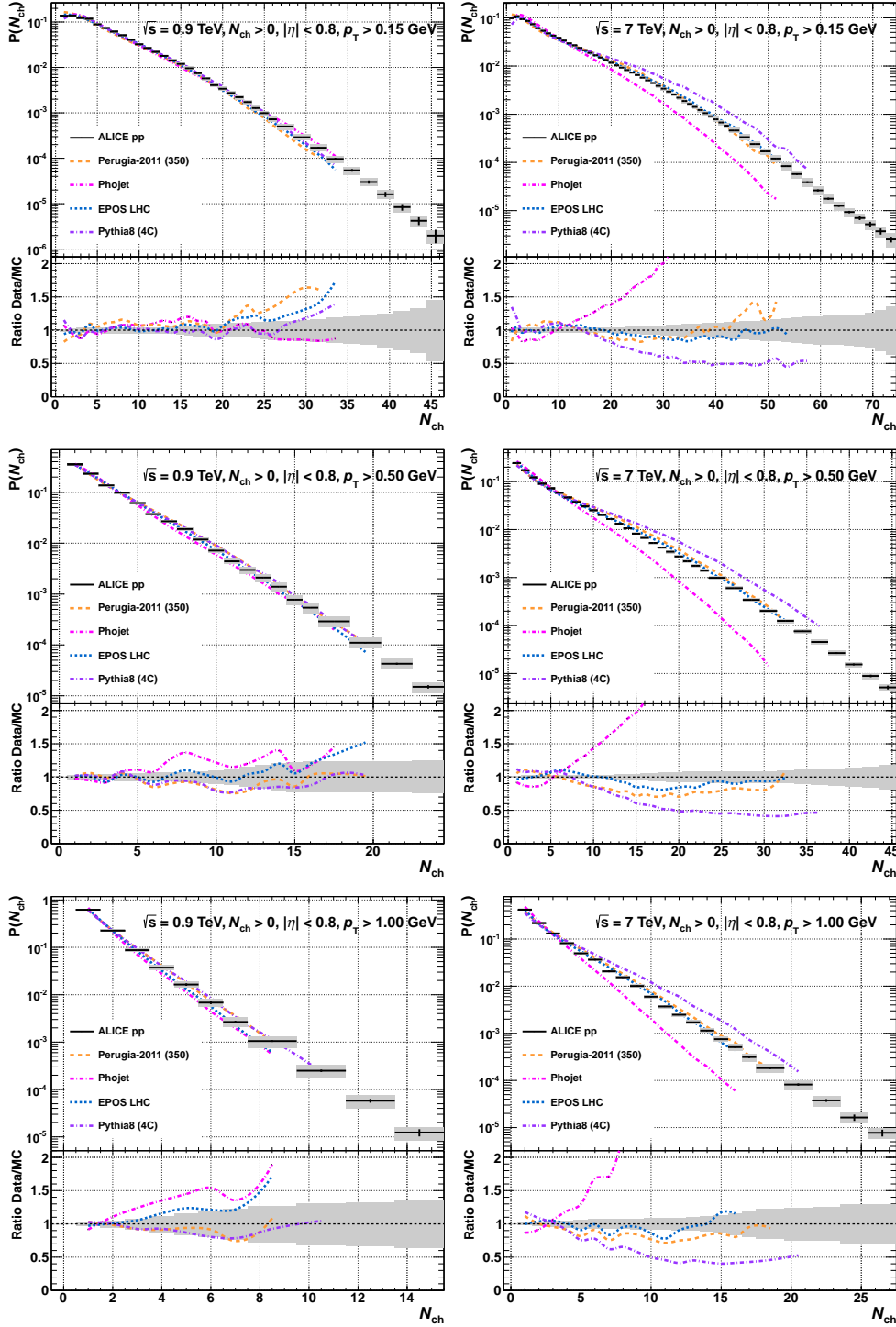


Fig. 12: Comparison with Monte Carlo predictions for the analysis at $\sqrt{s} = 0.9$ (left) and 7 TeV (right). The PYTHIA-6 Perugia-2011 tune is drawn, with the calculations from PHOJET, EPOS (LHC tune) and tune 4C of PYTHIA-8 (see text for references). The $p_{T,\text{cut}}$ is 0.15, 0.5, 1.0 GeV/c from top to bottom. In the upper panels, data are showed with both the statistical (black line) and systematic (grey band) uncertainties. The grey bands in the lower panels, where the ratios data/Monte Carlo are presented, correspond the total uncertainty on the final results. The wiggles in the ratios are due to interpolations between the points at various multiplicities. The Monte Carlo calculations are showed only in the range where their statistical uncertainty did not exceed 10%.

6 Conclusions

The charged particle pseudorapidity density and multiplicity distributions measured by ALICE with charged tracks reconstructed in the ITS and TPC detectors have been presented. The analyses were carried out using data collected in 2009 and 2010 at $\sqrt{s} = 0.9$ and 7 TeV. A $p_{T,\text{cut}}$ was used in order to characterize the class of events to be considered for the analysis, namely the $\text{INEL} > 0_{|\eta| < 0.8, p_{T} > p_{T,\text{cut}}}$ class, defined requiring at least one charged particle with $p_t > p_{T,\text{cut}}$ in $|\eta| < 0.8$. Three $p_{T,\text{cut}}$ values were used, 0.15, 0.5 and 1.0 GeV/ c . While the lowest $p_{T,\text{cut}}$ allows the most inclusive measurement for ALICE with global tracks, the 0.5 and 1.0 GeV/ c cuts were chosen together with the other LHC collaborations (ATLAS, CMS) to allow for the comparison with their results. The results were compared to different Monte Carlo models, showing that, with the striking exception of the LHC tune of EPOS, the selected Monte Carlo generators do not reproduce the measurements at both centre-of-mass energies and for all choices of $p_{T,\text{cut}}$.

References

- [1] K. Aamodt *et al.* [ALICE Collaboration], Eur. Phys. J. C **65** (2010) 111, arXiv:0911.5430 [hep-ex].
- [2] K. Aamodt *et al.* [ALICE Collaboration], Eur. Phys. J. C **68** (2010) 89 [arXiv:1004.3034 [hep-ex]].
- [3] K. Aamodt *et al.* [ALICE Collaboration], Eur. Phys. J. C **68** (2010) 345 [arXiv:1004.3514 [hep-ex]].
- [4] http://lpsc.web.cern.ch/LPCC/index.php?page=mb_ue_wg.
- [5] K. Aamodt *et al.* [ALICE Collaboration], Phys. Lett. B **693** (2010) 53 [arXiv:1007.0719 [hep-ex]].
- [6] J. F. Grosse-Oetringhaus, PhD thesis, University of Münster, Germany (2009). CERN-THESIS-2009-033.
- [7] F. Carminati *et al.*, ALICE Collaboration, Physics Performance Report Vol. I, CERN/LHCC 2003-049 and J. Phys. **G30** 1517 (2003); B. Alessandro *et al.*, ALICE Collaboration, Physics Performance Report Vol. II, CERN/LHCC 2005-030 and J. Phys. **G32** 1295 (2006); K. Aamodt *et al.*, ALICE Collaboration, JINST **3** (2008) S08002.
- [8] M. G. Albrow *et al.* (Tev4LHC QCD Working Group), arXiv:hep-ph/0610012 (2006). D6T (109) tune.
- [9] P. Z. Skands, in *Multi-Parton Interaction Workshop*, Perugia, Italy, 28-31 Oct. 2008, arXiv:0905.3418 [hep-ph] (2009).
- [10] B. Alessandro *et al.* [ALICE Collaboration], J. Phys. G: Nucl. Part. Phys. **32** (2006) 1295.
- [11] P. Billoir, Nucl. Instrum. Meth. A **225** (1984) 352.
- [12] E. Bruna *et al.*, ALICE Note, ALICE-INT-2009-018 (2009).
- [13] B. Abelev *et al.* [ALICE Collaboration], JHEP **1207** (2012) 116 [arXiv:1112.2082 [hep-ex]].
- [14] A. Moraes [ATLAS Collaboration], ATLAS Note ATL-COM-PHYS-2009-119 (2009). ATLAS CSC (306) tune.
- [15] V. Blobel in *8th CERN School of Comp., CSC84*, Aiguablava, Spain, 9-22 Sep. 1984, CERN-85-09, 88 (1985).
- [16] B. Abelev *et al.* [ALICE Collaboration], [arXiv:1208.4968 [hep-ex]].
- [17] R. Engel, J. Ranft, S. Roesler, Phys. Rev. D **52**, 1459 (1995).
- [18] G. Cowan, in *Advanced statistical techniques in particle physics*, Proceedings, Conference, Durham, UK, March 18-22, 2002, published in Conf. Proc. C **0203181** (2002) 248.
- [19] R. Field, *Min-Bias and the Underlying Event at the Tevatron and the LHC*, Fermilab ME/MC Tuning Workshop, Fermilab, Oct. 4, 2002.
- [20] P. Z. Skands, Phys. Rev. D **82** (2010) 074018 [arXiv:1005.3457 [hep-ph]].
- [21] T. Sjöstrand, S. Mrenna, P. Z. Skands, arXiv:0710.3820, CERN-LCGAPP-2007-04, LU TP 07-28,

FERMILAB-PUB-07-512-CD-T (2007).

- [22] R. Corke and T. Sjöstrand, JHEP **1103** (2011) 032 [arXiv:1011.1759 [hep-ph]].
- [23] K. Werner, F.-M. Liu and T. Pierog, Phys. Rev. C **74** (2006) 044902 [hep-ph/0506232]; T. Pierog, I. Karpenko, J. M. Katzy, E. Yatsenko and K. Werner, arXiv:1306.0121 [hep-ph].
- [24] [ATLAS Collaboration], ATLAS-CONF-2010-101.
- [25] Private communication.
- [26] [CMS Collaboration], CMS-PAS-QCD-10-004.

7 Acknowledgements

The ALICE collaboration would like to thank all its engineers and technicians for their invaluable contributions to the construction of the experiment and the CERN accelerator teams for the outstanding performance of the LHC complex.

The ALICE collaboration acknowledges the following funding agencies for their support in building and running the ALICE detector:

State Committee of Science, World Federation of Scientists (WFS) and Swiss Fonds Kidagan, Armenia, Conselho Nacional de Desenvolvimento Científico e Tecnológico (CNPq), Financiadora de Estudos e Projetos (FINEP), Fundação de Amparo à Pesquisa do Estado de São Paulo (FAPESP);

National Natural Science Foundation of China (NSFC), the Chinese Ministry of Education (CMOE) and the Ministry of Science and Technology of China (MSTC);

Ministry of Education and Youth of the Czech Republic;

Danish Natural Science Research Council, the Carlsberg Foundation and the Danish National Research Foundation;

The European Research Council under the European Community's Seventh Framework Programme;

Helsinki Institute of Physics and the Academy of Finland;

French CNRS-IN2P3, the 'Region Pays de Loire', 'Region Alsace', 'Region Auvergne' and CEA, France;

German BMBF and the Helmholtz Association;

General Secretariat for Research and Technology, Ministry of Development, Greece;

Hungarian OTKA and National Office for Research and Technology (NKTH);

Department of Atomic Energy and Department of Science and Technology of the Government of India;

Istituto Nazionale di Fisica Nucleare (INFN) and Centro Fermi - Museo Storico della Fisica e Centro Studi e Ricerche "Enrico Fermi", Italy;

MEXT Grant-in-Aid for Specially Promoted Research, Japan;

Joint Institute for Nuclear Research, Dubna;

National Research Foundation of Korea (NRF);

CONACYT, DGAPA, México, ALFA-EC and the EPLANET Program (European Particle Physics Latin American Network)

Stichting voor Fundamenteel Onderzoek der Materie (FOM) and the Nederlandse Organisatie voor Wetenschappelijk Onderzoek (NWO), Netherlands;

Research Council of Norway (NFR);

Polish Ministry of Science and Higher Education;

National Authority for Scientific Research - NASR (Autoritatea Națională pentru Cercetare Științifică - ANCS);

Ministry of Education and Science of Russian Federation, Russian Academy of Sciences, Russian Federal Agency of Atomic Energy, Russian Federal Agency for Science and Innovations and The Russian Foundation for Basic Research;

Ministry of Education of Slovakia;

Department of Science and Technology, South Africa;

CIEMAT, EELA, Ministerio de Economía y Competitividad (MINECO) of Spain, Xunta de Galicia (Consellería de Educación), CEADEN, Cubaenergía, Cuba, and IAEA (International Atomic Energy Agency);

Swedish Research Council (VR) and Knut & Alice Wallenberg Foundation (KAW);

Ukraine Ministry of Education and Science;

United Kingdom Science and Technology Facilities Council (STFC);

The United States Department of Energy, the United States National Science Foundation, the State of Texas, and the State of Ohio.

A The ALICE Collaboration

B. Abelev⁶⁹, J. Adam³⁶, D. Adamová⁷⁷, A.M. Adare¹²⁵, M.M. Aggarwal⁸¹, G. Aglieri Rinella³³, M. Agnello^{87,104}, A.G. Agocs¹²⁴, A. Agostinelli²⁵, Z. Ahammed¹²⁰, N. Ahmad¹⁶, A. Ahmad Masoodi¹⁶, I. Ahmed¹⁴, S.U. Ahn⁶², S.A. Ahn⁶², I. Aimo^{104,87}, S. Aiola¹²⁵, M. Ajaz¹⁴, A. Akindinov⁵³, D. Aleksandrov⁹³, B. Alessandro¹⁰⁴, D. Alexandre⁹⁵, A. Alici^{11,98}, A. Alkin³, J. Alme³⁴, T. Alt³⁸, V. Altini³⁰, S. Altinpinar¹⁷, I. Altsybeev¹¹⁹, C. Alves Garcia Prado¹¹¹, C. Andrei⁷², A. Andronic⁹⁰, V. Anguelov⁸⁶, J. Anielski⁴⁸, T. Antičić⁹¹, F. Antinori¹⁰¹, P. Antonioli⁹⁸, L. Aphecetche¹⁰⁵, H. Appelshäuser⁴⁶, N. Arbor⁶⁵, S. Arcelli²⁵, N. Armesto¹⁵, R. Arnaldi¹⁰⁴, T. Aronsson¹²⁵, I.C. Arsene⁹⁰, M. Arslanok⁴⁶, A. Augustinus³³, R. Averbeck⁹⁰, T.C. Awes⁷⁸, M.D. Azmi⁸³, M. Bach³⁸, A. Badalà¹⁰⁰, Y.W. Baek^{64,39}, R. Bailhache⁴⁶, V. Bairathi⁸⁵, R. Bala^{104,84}, A. Baldisseri¹³, F. Baltasar Dos Santos Pedrosa³³, J. Bán⁵⁴, R.C. Baral⁵⁶, R. Barbera²⁶, F. Barile³⁰, G.G. Barnaföldi¹²⁴, L.S. Barnby⁹⁵, V. Barret⁶⁴, J. Bartke¹⁰⁸, M. Basile²⁵, N. Bastid⁶⁴, S. Basu¹²⁰, B. Bathen⁴⁸, G. Batigne¹⁰⁵, B. Batyunya⁶¹, P.C. Batzing²⁰, C. Baumann⁴⁶, I.G. Bearden⁷⁴, H. Beck⁴⁶, N.K. Behera⁴², I. Belikov⁴⁹, F. Bellini²⁵, R. Bellwied¹¹³, E. Belmont-Moreno⁵⁹, G. Bencedi¹²⁴, S. Beole²³, I. Berceau⁷², A. Bercuci⁷², Y. Berdnikov⁷⁹, D. Berenyi¹²⁴, A.A.E. Bergognon¹⁰⁵, R.A. Bertens⁵², D. Berzano²³, L. Betev³³, A. Bhasin⁸⁴, A.K. Bhati⁸¹, J. Bhom¹¹⁷, L. Bianchi²³, N. Bianchi⁶⁶, J. Bielčák³⁶, J. Bielčiková⁷⁷, A. Bilandžić⁷⁴, S. Bjelogrić⁵², F. Blanco⁹, F. Blanco¹¹³, D. Blau⁹³, C. Blume⁴⁶, F. Bock^{68,86}, A. Bogdanov⁷⁰, H. Bøggild⁷⁴, M. Bogolyubsky⁵⁰, L. Boldizsár¹²⁴, M. Bombara³⁷, J. Book⁴⁶, H. Borel¹³, A. Borissov¹²³, J. Bornschein³⁸, M. Botje⁷⁵, E. Botta²³, S. Böttger⁴⁵, P. Braun-Munzinger⁹⁰, M. Bregant¹⁰⁵, T. Breitner⁴⁵, T.A. Broker⁴⁶, T.A. Browning⁸⁸, M. Broz³⁵, R. Brun³³, E. Bruna¹⁰⁴, G.E. Bruno³⁰, D. Budnikov⁹², H. Buesching⁴⁶, S. Bufalino¹⁰⁴, P. Buncic³³, O. Busch⁸⁶, Z. Buthelezi⁶⁰, D. Caffarri²⁷, X. Cai⁶, H. Caines¹²⁵, A. Caliva⁵², E. Calvo Villar⁹⁶, P. Camerini²², V. Canoa Roman^{10,33}, G. Cara Romeo⁹⁸, F. Carena³³, W. Carena³³, F. Carminati³³, A. Casanova Díaz⁶⁶, J. Castillo Castellanos¹³, E.A.R. Casula²¹, V. Catanesu⁷², C. Cavicchioli³³, C. Ceballos Sanchez⁸, J. Cepila³⁶, P. Cerello¹⁰⁴, B. Chang¹¹⁴, S. Chapeland³³, J.L. Charvet¹³, S. Chattopadhyay¹²⁰, S. Chattopadhyay⁹⁴, M. Cherney⁸⁰, C. Cheshkov¹¹⁸, B. Cheynis¹¹⁸, V. Chibante Barroso³³, D.D. Chinellato¹¹³, P. Chochula³³, M. Chojnacki⁷⁴, S. Choudhury¹²⁰, P. Christakoglou⁷⁵, C.H. Christensen⁷⁴, P. Christiansen³¹, T. Chujo¹¹⁷, S.U. Chung⁸⁹, C. Cicalo⁹⁹, L. Cifarelli^{11,25}, F. Cindolo⁹⁸, J. Cleymans⁸³, F. Colamaria³⁰, D. Colella³⁰, A. Collu²¹, M. Colocci²⁵, G. Conesa Balbastre⁶⁵, Z. Conesa del Valle^{44,33}, M.E. Connors¹²⁵, G. Contin²², J.G. Contreras¹⁰, T.M. Cormier¹²³, Y. Corrales Morales²³, P. Cortese²⁹, I. Cortés Maldonado², M.R. Cosentino⁶⁸, F. Costa³³, P. Crochet⁶⁴, R. Cruz Albino¹⁰, E. Cuautle⁵⁸, L. Cunqueiro^{66,33}, A. Dainese¹⁰¹, R. Dang⁶, A. Danu⁵⁷, K. Das⁹⁴, D. Das⁹⁴, I. Das⁴⁴, A. Dash¹¹², S. Dash⁴², S. De¹²⁰, H. Delagrange¹⁰⁵, A. Deloff⁷¹, E. Dénes¹²⁴, A. Deppman¹¹¹, G.O.V. de Barros¹¹¹, A. De Caro^{11,28}, G. de Cataldo⁹⁷, J. de Cuveland³⁸, A. De Falco²¹, D. De Gruttola^{28,11}, N. De Marco¹⁰⁴, S. De Pasquale²⁸, R. de Rooij⁵², M.A. Diaz Corchero⁹, T. Dietel⁴⁸, R. Divià³³, D. Di Bari³⁰, C. Di Giglio³⁰, S. Di Liberto¹⁰², A. Di Mauro³³, P. Di Nezza⁶⁶, Ø. Djuvsland¹⁷, A. Dobrin^{52,123}, T. Dobrowolski⁷¹, B. Dönigus^{90,46}, O. Dordic²⁰, A.K. Dubey¹²⁰, A. Dubla⁵², L. Ducroux¹¹⁸, P. Dupieux⁶⁴, A.K. Dutta Majumdar⁹⁴, G. D'Erasmus³⁰, D. Elia⁹⁷, D. Emschermann⁴⁸, H. Engel⁴⁵, B. Erazmus^{33,105}, H.A. Erdal³⁴, D. Eschweiler³⁸, B. Espagnon⁴⁴, M. Estienne¹⁰⁵, S. Esumi¹¹⁷, D. Evans⁹⁵, S. Evdokimov⁵⁰, G. Eyyubova²⁰, D. Fabris¹⁰¹, J. Faivre⁶⁵, D. Falchieri²⁵, A. Fantoni⁶⁶, M. Fasel⁸⁶, D. Fehlker¹⁷, L. Feldkamp⁴⁸, D. Felea⁵⁷, A. Feliciello¹⁰⁴, G. Feofilov¹¹⁹, J. Ferencei⁷⁷, A. Fernández Téllez², E.G. Ferreira¹⁵, A. Ferretti²³, A. Festanti²⁷, J. Figiel¹⁰⁸, M.A.S. Figueredo¹¹¹, S. Filchagin⁹², D. Finogeev⁵¹, F.M. Fionda³⁰, E.M. Fiore³⁰, E. Floratos⁸², M. Floris³³, S. Foertsch⁶⁰, P. Foka⁹⁰, S. Fokin⁹³, E. Fragiaco¹⁰³, A. Francescon^{27,33}, U. Frankenfeld⁹⁰, U. Fuchs³³, C. Furget⁶⁵, M. Fusco Girard²⁸, J.J. Gaardhøje⁷⁴, M. Gagliardi²³, A. Gago⁹⁶, M. Gallio²³, D.R. Gangadharan¹⁸, P. Ganoti⁷⁸, C. Garabatos⁹⁰, E. Garcia-Solis¹², C. Gargiulo³³, I. Garishvili⁶⁹, J. Gerhard³⁸, M. Germain¹⁰⁵, A. Gheata³³, M. Gheata^{33,57}, B. Ghidini³⁰, P. Ghosh¹²⁰, P. Gianotti⁶⁶, P. Giubellino³³, E. Gladysz-Dziadus¹⁰⁸, P. Glässel⁸⁶, L. Goerlich¹⁰⁸, R. Gomez^{10,110}, P. González-Zamora⁹, S. Gorbunov³⁸, S. Gotovac¹⁰⁷, L.K. Graczykowski¹²², R. Grajcarek⁸⁶, A. Grelli⁵², C. Grigoras³³, A. Grigoras³³, V. Grigoriev⁷⁰, A. Grigoryan¹, S. Grigoryan⁶¹, B. Grinyov³, N. Grion¹⁰³, J.F. Grosse-Oetringhaus³³, J.-Y. Grossiord¹¹⁸, R. Grosso³³, F. Guber⁵¹, R. Guernane⁶⁵, B. Guerzoni²⁵, M. Guilbaud¹¹⁸, K. Gulbrandsen⁷⁴, H. Gulkanyan¹, T. Gunji¹¹⁶, A. Gupta⁸⁴, R. Gupta⁸⁴, K. H. Khan¹⁴, R. Haake⁴⁸, Ø. Haaland¹⁷, C. Hadjidakis⁴⁴, M. Haiduc⁵⁷, H. Hamagaki¹¹⁶, G. Hamar¹²⁴, L.D. Hanratty⁹⁵, A. Hansen⁷⁴, J.W. Harris¹²⁵, H. Hartmann³⁸, A. Harton¹², D. Hatzifotiadou⁹⁸, S. Hayashi¹¹⁶, A. Hayrapetyan^{33,1}, S.T. Heckel⁴⁶, M. Heide⁴⁸, H. Helstrup³⁴, A. Herghelegiu⁷², G. Herrera Corral¹⁰, N. Herrmann⁸⁶, B.A. Hess³², K.F. Hetland³⁴, B. Hicks¹²⁵, B. Hippolyte⁴⁹, Y. Hori¹¹⁶, P. Hristov³³, I. Hrivnáčová⁴⁴, M. Huang¹⁷, T.J. Humanic¹⁸, D. Hutter³⁸, D.S. Hwang¹⁹, R. Ilkaev⁹², I. Ilkiv⁷¹, M. Inaba¹¹⁷, E. Incani²¹, G.M. Innocenti²³, C. Ionita³³, M. Ippolitov⁹³, M. Irfan¹⁶, M. Ivanov⁹⁰, V. Ivanov⁷⁹,

O. Ivanytskyi³, A. Jachołkowski²⁶, C. Jahnke¹¹¹, H.J. Jang⁶², M.A. Janik¹²², P.H.S.Y. Jayarathna¹¹³, S. Jena^{42,113}, R.T. Jimenez Bustamante⁵⁸, P.G. Jones⁹⁵, H. Jung³⁹, A. Jusko⁹⁵, S. Kalcher³⁸, P. Kaliňák⁵⁴, A. Kalweit³³, J.H. Kang¹²⁶, V. Kaplin⁷⁰, S. Kar¹²⁰, A. Karasu Uysal⁶³, O. Karavichev⁵¹, T. Karavicheva⁵¹, E. Karpechev⁵¹, A. Kazantsev⁹³, U. Kebschull⁴⁵, R. Keidel¹²⁷, B. Ketzer⁴⁶, M.M. Khan¹⁶, P. Khan⁹⁴, S.A. Khan¹²⁰, A. Khanzadeev⁷⁹, Y. Kharlov⁵⁰, B. Kileng³⁴, T. Kim¹²⁶, B. Kim¹²⁶, D.J. Kim¹¹⁴, D.W. Kim^{39,62}, J.S. Kim³⁹, M. Kim³⁹, M. Kim¹²⁶, S. Kim¹⁹, S. Kirsch³⁸, I. Kisel³⁸, S. Kiselev⁵³, A. Kisiel¹²², G. Kiss¹²⁴, J.L. Klay⁵, J. Klein⁸⁶, C. Klein-Bösing⁴⁸, A. Kluge³³, M.L. Knichel⁹⁰, A.G. Knospe¹⁰⁹, C. Kobdaj^{33,106}, M.K. Köhler⁹⁰, T. Kollegger³⁸, A. Kolojvari¹¹⁹, V. Kondratiev¹¹⁹, N. Kondratyeva⁷⁰, A. Konevskikh⁵¹, V. Kovalenko¹¹⁹, M. Kowalski¹⁰⁸, S. Kox⁶⁵, G. Koyithatta Meethalevedu⁴², J. Kral¹¹⁴, I. Králik⁵⁴, F. Kramer⁴⁶, A. Kravčáková³⁷, M. Krelina³⁶, M. Kretz³⁸, M. Krivda^{54,95}, F. Krizek^{36,77,40}, M. Krus³⁶, E. Kryshen⁷⁹, M. Krzewicki⁹⁰, V. Kucera⁷⁷, Y. Kucheriaev⁹³, T. Kugathasan³³, C. Kuhn⁴⁹, P.G. Kuijjer⁷⁵, I. Kulakov⁴⁶, J. Kumar⁴², P. Kurashvili⁷¹, A.B. Kurepin⁵¹, A. Kurepin⁵¹, A. Kuryakin⁹², V. Kushpil⁷⁷, S. Kushpil⁷⁷, M.J. Kweon⁸⁶, Y. Kwon¹²⁶, P. Ladrón de Guevara⁵⁸, C. Lagana Fernandes¹¹¹, I. Lakomov⁴⁴, R. Langoy¹²¹, C. Lara⁴⁵, A. Lardeux¹⁰⁵, A. Lattuca²³, S.L. La Pointe⁵², P. La Rocca²⁶, R. Lea²², M. Lechman³³, S.C. Lee³⁹, G.R. Lee⁹⁵, I. Legrand³³, J. Lehnert⁴⁶, R.C. Lemmon⁷⁶, M. Lenhardt⁹⁰, V. Lenti⁹⁷, M. Leoncino²³, I. León Monzón¹¹⁰, P. Lévai¹²⁴, S. Li^{64,6}, J. Lien^{121,17}, R. Lietava⁹⁵, S. Lindal²⁰, V. Lindenstruth³⁸, C. Lippmann⁹⁰, M.A. Lisa¹⁸, H.M. Ljunggren³¹, D.F. Lodato⁵², P.I. Loenne¹⁷, V.R. Loggins¹²³, V. Loginov⁷⁰, D. Lohner⁸⁶, C. Loizides⁶⁸, X. Lopez⁶⁴, E. López Torres⁸, G. Løvnhøiden²⁰, X.-G. Lu⁸⁶, P. Luettig⁴⁶, M. Lunardon²⁷, J. Luo⁶, G. Luparello⁵², C. Luzzi³³, P. M. Jacobs⁶⁸, R. Ma¹²⁵, A. Maevskaya⁵¹, M. Mager³³, D.P. Mahapatra⁵⁶, A. Maire⁸⁶, M. Malaev⁷⁹, I. Maldonado Cervantes⁵⁸, L. Malinina^{61,ii}, D. Mal'Kevich⁵³, P. Malzacher⁹⁰, A. Mamonov⁹², L. Manceau¹⁰⁴, V. Manko⁹³, F. Manso⁶⁴, V. Manzari^{97,33}, M. Marchisone^{64,23}, J. Mareš⁵⁵, G.V. Margagliotti²², A. Margotti⁹⁸, A. Marín⁹⁰, C. Markert^{109,33}, M. Marquard⁴⁶, I. Martashvili¹¹⁵, N.A. Martin⁹⁰, P. Martinengo³³, M.I. Martínez², G. Martínez García¹⁰⁵, J. Martin Blanco¹⁰⁵, Y. Martynov³, A. Mas¹⁰⁵, S. Masciocchi⁹⁰, M. Maserà²³, A. Masoni⁹⁹, L. Massacrier¹⁰⁵, A. Mastroserio³⁰, A. Matyja¹⁰⁸, J. Mazer¹¹⁵, R. Mazumder⁴³, M.A. Mazzoni¹⁰², F. Meddi²⁴, A. Menchaca-Rocha⁵⁹, J. Mercado Pérez⁸⁶, M. Meres³⁵, Y. Miake¹¹⁷, K. Mikhaylov^{61,53}, L. Milano^{33,23}, J. Milosevic^{20,iii}, A. Mischke⁵², A.N. Mishra⁴³, D. Miśkowiec⁹⁰, C. Mitu⁵⁷, J. Mlynar¹²³, B. Mohanty^{120,73}, L. Molnar^{49,124}, L. Montaña Zetina¹⁰, M. Monteno¹⁰⁴, E. Montes⁹, M. Morando²⁷, D.A. Moreira De Godoy¹¹¹, S. Moretto²⁷, A. Morreale¹¹⁴, A. Morsch³³, V. Muccifora⁶⁶, E. Mudnic¹⁰⁷, S. Muhuri¹²⁰, M. Mukherjee¹²⁰, H. Müller³³, M.G. Munhoz¹¹¹, S. Murray⁶⁰, L. Musa³³, B.K. Nandi⁴², R. Nania⁹⁸, E. Nappi⁹⁷, C. Natrass¹¹⁵, T.K. Nayak¹²⁰, S. Nazarenko⁹², A. Nedosekin⁵³, M. Nicassio^{90,30}, M. Niculescu^{33,57}, B.S. Nielsen⁷⁴, S. Nikolaev⁹³, S. Nikulin⁹³, V. Nikulin⁷⁹, B.S. Nilsen⁸⁰, M.S. Nilsson²⁰, F. Noferini^{11,98}, P. Nomokonov⁶¹, G. Nooren⁵², A. Nyanin⁹³, A. Nyatha⁴², J. Nystrand¹⁷, H. Oeschler^{86,47}, S.K. Oh^{39,iv}, S. Oh¹²⁵, L. Olah¹²⁴, J. Oleniacz¹²², A.C. Oliveira Da Silva¹¹¹, J. Onderwaater⁹⁰, C. Oppedisano¹⁰⁴, A. Ortiz Velasquez³¹, A. Oskarsson³¹, J. Otwinowski⁹⁰, K. Oyama⁸⁶, Y. Pachmayer⁸⁶, M. Pachr³⁶, P. Pagano²⁸, G. Paic⁵⁸, F. Painke³⁸, C. Pajares¹⁵, S.K. Pal¹²⁰, A. Palaha⁹⁵, A. Palmeri¹⁰⁰, V. Papikyan¹, G.S. Pappalardo¹⁰⁰, W.J. Park⁹⁰, A. Passfeld⁴⁸, D.I. Patalakha⁵⁰, V. Paticchio⁹⁷, B. Paul⁹⁴, T. Pawlak¹²², T. Peitzmann⁵², H. Pereira Da Costa¹³, E. Pereira De Oliveira Filho¹¹¹, D. Peresunko⁹³, C.E. Pérez Lara⁷⁵, D. Perrino³⁰, W. Peryt^{122,i}, A. Pesci⁹⁸, Y. Pestov⁴, V. Petráček³⁶, M. Petran³⁶, M. Petris⁷², P. Petrov⁹⁵, M. Petrovici⁷², C. Petta²⁶, S. Piano¹⁰³, M. Pikna³⁵, P. Pillot¹⁰⁵, O. Pinazza^{33,98}, L. Pinsky¹¹³, N. Pitz⁴⁶, D.B. Piyarathna¹¹³, M. Planinic⁹¹, M. Płoskoń⁶⁸, J. Pluta¹²², S. Pochybova¹²⁴, P.L.M. Podesta-Lerma¹¹⁰, M.G. Poghosyan³³, B. Polichtchouk⁵⁰, A. Pop⁷², S. Porteboeuf-Houssais⁶⁴, V. Pospíšil³⁶, B. Potukuchi⁸⁴, S.K. Prasad¹²³, R. Preghenella^{11,98}, F. Prino¹⁰⁴, C.A. Pruneau¹²³, I. Pshenichnov⁵¹, G. Puddu²¹, V. Punin⁹², J. Putschke¹²³, H. Qvigstad²⁰, A. Rachevski¹⁰³, A. Rademakers³³, J. Rak¹¹⁴, A. Rakotozafindrabe¹³, L. Ramello²⁹, S. Raniwala⁸⁵, R. Raniwala⁸⁵, S.S. Räsänen⁴⁰, B.T. Rascanu⁴⁶, D. Rathee⁸¹, W. Rauch³³, A.W. Rauf¹⁴, V. Razazi²¹, K.F. Read¹¹⁵, J.S. Real⁶⁵, K. Redlich^{71,v}, R.J. Reed¹²⁵, A. Rehman¹⁷, P. Reichelt⁴⁶, M. Reicher⁵², F. Reidt^{33,86}, R. Renfordt⁴⁶, A.R. Reolon⁶⁶, A. Reshetin⁵¹, F. Rettig³⁸, J.-P. Revol³³, K. Reygers⁸⁶, L. Riccati¹⁰⁴, R.A. Ricci⁶⁷, T. Richert³¹, M. Richter²⁰, P. Riedler³³, W. Riegler³³, F. Riggi²⁶, A. Rivetti¹⁰⁴, M. Rodríguez Cahuantzi², A. Rodríguez Manso⁷⁵, K. Røed^{17,20}, E. Rogochaya⁶¹, S. Rohni⁸⁴, D. Rohr³⁸, D. Röhrich¹⁷, R. Romita^{76,90}, F. Ronchetti⁶⁶, P. Rosnet⁶⁴, S. Rossegger³³, A. Rossi³³, P. Roy⁹⁴, C. Roy⁴⁹, A.J. Rubio Montero⁹, R. Rui²², R. Russo²³, E. Ryabinkin⁹³, A. Rybicki¹⁰⁸, S. Sadovsky⁵⁰, K. Šafařík³³, R. Sahoo⁴³, P.K. Sahu⁵⁶, J. Saini¹²⁰, H. Sakaguchi⁴¹, S. Sakai^{68,66}, D. Sakata¹¹⁷, C.A. Salgado¹⁵, J. Salzwedel¹⁸, S. Sambyal⁸⁴, V. Samsonov⁷⁹, X. Sanchez Castro^{58,49}, L. Šándor⁵⁴, A. Sandoval⁵⁹, M. Sano¹¹⁷, G. Santagati²⁶, R. Santoro^{11,33}, D. Sarkar¹²⁰, E. Scapparone⁹⁸, F. Scarlassara²⁷, R.P. Scharenberg⁸⁸, C. Schiaua⁷², R. Schicker⁸⁶, C. Schmidt⁹⁰, H.R. Schmidt³², S. Schuchmann⁴⁶,

J. Schukraft³³, M. Schulc³⁶, T. Schuster¹²⁵, Y. Schutz^{33,105}, K. Schwarz⁹⁰, K. Schweda⁹⁰, G. Scioli²⁵, E. Scomparin¹⁰⁴, R. Scott¹¹⁵, P.A. Scott⁹⁵, G. Segato²⁷, I. Selyuzhenkov⁹⁰, J. Seo⁸⁹, S. Serici²¹, E. Serradilla^{9,59}, A. Sevcenco⁵⁷, A. Shabetai¹⁰⁵, G. Shabratova⁶¹, R. Shahoyan³³, S. Sharma⁸⁴, N. Sharma¹¹⁵, K. Shigaki⁴¹, K. Shtejer⁸, Y. Sibiriak⁹³, S. Siddhanta⁹⁹, T. Siemiarczuk⁷¹, D. Silvermyr⁷⁸, C. Silvestre⁶⁵, G. Simatovic⁹¹, R. Singaraju¹²⁰, R. Singh⁸⁴, S. Singha¹²⁰, V. Singhal¹²⁰, B.C. Sinha¹²⁰, T. Sinha⁹⁴, B. Sitar³⁵, M. Sitta²⁹, T.B. Skaali²⁰, K. Skjerdal¹⁷, R. Smakal³⁶, N. Smirnov¹²⁵, R.J.M. Snellings⁵², R. Soltz⁶⁹, M. Song¹²⁶, J. Song⁸⁹, C. Soos³³, F. Soramel²⁷, M. Spacek³⁶, I. Sputowska¹⁰⁸, M. Spyropoulou-Stassinaki⁸², B.K. Srivastava⁸⁸, J. Stachel⁸⁶, I. Stan⁵⁷, G. Stefanek⁷¹, M. Steinpreis¹⁸, E. Stenlund³¹, G. Steyn⁶⁰, J.H. Stiller⁸⁶, D. Stocco¹⁰⁵, M. Stolpovskiy⁵⁰, P. Strmen³⁵, A.A.P. Suaide¹¹¹, M.A. Subieta Vásquez²³, T. Sugitate⁴¹, C. Suire⁴⁴, M. Suleymanov¹⁴, R. Sultanov⁵³, M. Šumbera⁷⁷, T. Susa⁹¹, T.J.M. Symons⁶⁸, A. Szanto de Toledo¹¹¹, I. Szarka³⁵, A. Szczepankiewicz³³, M. Szymański¹²², J. Takahashi¹¹², M.A. Tangaro³⁰, J.D. Tapia Takaki⁴⁴, A. Tarantola Peloni⁴⁶, A. Tarazona Martinez³³, A. Tauro³³, G. Tejada Muñoz², A. Telesca³³, C. Terrevoli³⁰, A. Ter Minasyan^{93,70}, J. Thäder⁹⁰, D. Thomas⁵², R. Tieulent¹¹⁸, A.R. Timmins¹¹³, A. Toia¹⁰¹, H. Torii¹¹⁶, V. Trubnikov³, W.H. Trzaska¹¹⁴, T. Tsuji¹¹⁶, A. Tumkin⁹², R. Turrisi¹⁰¹, T.S. Tveter²⁰, J. Ulery⁴⁶, K. Ullaland¹⁷, J. Ulrich⁴⁵, A. Uras¹¹⁸, G.M. Urciuoli¹⁰², G.L. Usai²¹, M. Vajzer⁷⁷, M. Vala^{54,61}, L. Valencia Palomo⁴⁴, P. Vande Vyvre³³, L. Vannucci⁶⁷, J.W. Van Hoorne³³, M. van Leeuwen⁵², A. Vargas², R. Varma⁴², M. Vasileiou⁸², A. Vasiliev⁹³, V. Vechernin¹¹⁹, M. Veldhoen⁵², M. Venaruzzo²², E. Vercellin²³, S. Vergara², R. Vernet⁷, M. Verweij^{123,52}, L. Vickovic¹⁰⁷, G. Viesti²⁷, J. Viinikainen¹¹⁴, Z. Vilakazi⁶⁰, O. Villalobos Baillie⁹⁵, A. Vinogradov⁹³, L. Vinogradov¹¹⁹, Y. Vinogradov⁹², T. Virgili²⁸, Y.P. Viyogi¹²⁰, A. Vodopyanov⁶¹, M.A. Völkl⁸⁶, S. Voloshin¹²³, K. Voloshin⁵³, G. Volpe³³, B. von Haller³³, I. Vorobyev¹¹⁹, D. Vranic^{33,90}, J. Vrláková³⁷, B. Vulpescu⁶⁴, A. Vyushin⁹², B. Wagner¹⁷, V. Wagner³⁶, J. Wagner⁹⁰, Y. Wang⁸⁶, Y. Wang⁶, M. Wang⁶, D. Watanabe¹¹⁷, K. Watanabe¹¹⁷, M. Weber¹¹³, J.P. Wessels⁴⁸, U. Westerhoff⁴⁸, J. Wiechula³², J. Wikne²⁰, M. Wilde⁴⁸, G. Wilk⁷¹, J. Wilkinson⁸⁶, M.C.S. Williams⁹⁸, B. Windelband⁸⁶, M. Winn⁸⁶, C. Xiang⁶, C.G. Yaldo¹²³, Y. Yamaguchi¹¹⁶, H. Yang^{13,52}, P. Yang⁶, S. Yang¹⁷, S. Yano⁴¹, S. Yasnopolskiy⁹³, J. Yi⁸⁹, Z. Yin⁶, I.-K. Yoo⁸⁹, I. Yushmanov⁹³, V. Zaccolo⁷⁴, C. Zach³⁶, C. Zampolli⁹⁸, S. Zaporozhets⁶¹, A. Zarochentsev¹¹⁹, P. Závada⁵⁵, N. Zaviyalov⁹², H. Zbroszczyk¹²², P. Zelniczek⁴⁵, I.S. Zgura⁵⁷, M. Zhalov⁷⁹, F. Zhang⁶, Y. Zhang⁶, H. Zhang⁶, X. Zhang^{68,64,6}, D. Zhou⁶, Y. Zhou⁵², F. Zhou⁶, X. Zhu⁶, J. Zhu⁶, H. Zhu⁶, A. Zichichi^{11,25}, M.B. Zimmermann^{48,33}, A. Zimmermann⁸⁶, G. Zinovjev³, Y. Zoccarato¹¹⁸, M. Zynovyev³, M. Zyzak⁴⁶

Affiliation notes

ⁱ Deceased

ⁱⁱ Also at: M.V.Lomonosov Moscow State University, D.V.Skobeltsyn Institute of Nuclear Physics, Moscow, Russia

ⁱⁱⁱ Also at: University of Belgrade, Faculty of Physics and "Vinča" Institute of Nuclear Sciences, Belgrade, Serbia

^{iv} Permanent address: Konkuk University, Seoul, Korea

^v Also at: Institute of Theoretical Physics, University of Wrocław, Wrocław, Poland

Collaboration Institutes

¹ A. I. Alikhanyan National Science Laboratory (Yerevan Physics Institute) Foundation, Yerevan, Armenia

² Benemérita Universidad Autónoma de Puebla, Puebla, Mexico

³ Bogolyubov Institute for Theoretical Physics, Kiev, Ukraine

⁴ Budker Institute for Nuclear Physics, Novosibirsk, Russia

⁵ California Polytechnic State University, San Luis Obispo, California, United States

⁶ Central China Normal University, Wuhan, China

⁷ Centre de Calcul de l'IN2P3, Villeurbanne, France

⁸ Centro de Aplicaciones Tecnológicas y Desarrollo Nuclear (CEADEN), Havana, Cuba

⁹ Centro de Investigaciones Energéticas Medioambientales y Tecnológicas (CIEMAT), Madrid, Spain

¹⁰ Centro de Investigación y de Estudios Avanzados (CINVESTAV), Mexico City and Mérida, Mexico

¹¹ Centro Fermi - Museo Storico della Fisica e Centro Studi e Ricerche "Enrico Fermi", Rome, Italy

¹² Chicago State University, Chicago, United States

¹³ Commissariat à l'Énergie Atomique, IRFU, Saclay, France

¹⁴ COMSATS Institute of Information Technology (CIIT), Islamabad, Pakistan

- 15 Departamento de Física de Partículas and IGFAE, Universidad de Santiago de Compostela, Santiago de Compostela, Spain
- 16 Department of Physics Aligarh Muslim University, Aligarh, India
- 17 Department of Physics and Technology, University of Bergen, Bergen, Norway
- 18 Department of Physics, Ohio State University, Columbus, Ohio, United States
- 19 Department of Physics, Sejong University, Seoul, South Korea
- 20 Department of Physics, University of Oslo, Oslo, Norway
- 21 Dipartimento di Fisica dell'Università and Sezione INFN, Cagliari, Italy
- 22 Dipartimento di Fisica dell'Università and Sezione INFN, Trieste, Italy
- 23 Dipartimento di Fisica dell'Università and Sezione INFN, Turin, Italy
- 24 Dipartimento di Fisica dell'Università 'La Sapienza' and Sezione INFN, Rome, Italy
- 25 Dipartimento di Fisica e Astronomia dell'Università and Sezione INFN, Bologna, Italy
- 26 Dipartimento di Fisica e Astronomia dell'Università and Sezione INFN, Catania, Italy
- 27 Dipartimento di Fisica e Astronomia dell'Università and Sezione INFN, Padova, Italy
- 28 Dipartimento di Fisica 'E.R. Caianiello' dell'Università and Gruppo Collegato INFN, Salerno, Italy
- 29 Dipartimento di Scienze e Innovazione Tecnologica dell'Università del Piemonte Orientale and Gruppo Collegato INFN, Alessandria, Italy
- 30 Dipartimento Interateneo di Fisica 'M. Merlin' and Sezione INFN, Bari, Italy
- 31 Division of Experimental High Energy Physics, University of Lund, Lund, Sweden
- 32 Eberhard Karls Universität Tübingen, Tübingen, Germany
- 33 European Organization for Nuclear Research (CERN), Geneva, Switzerland
- 34 Faculty of Engineering, Bergen University College, Bergen, Norway
- 35 Faculty of Mathematics, Physics and Informatics, Comenius University, Bratislava, Slovakia
- 36 Faculty of Nuclear Sciences and Physical Engineering, Czech Technical University in Prague, Prague, Czech Republic
- 37 Faculty of Science, P.J. Šafárik University, Košice, Slovakia
- 38 Frankfurt Institute for Advanced Studies, Johann Wolfgang Goethe-Universität Frankfurt, Frankfurt, Germany
- 39 Gangneung-Wonju National University, Gangneung, South Korea
- 40 Helsinki Institute of Physics (HIP), Helsinki, Finland
- 41 Hiroshima University, Hiroshima, Japan
- 42 Indian Institute of Technology Bombay (IIT), Mumbai, India
- 43 Indian Institute of Technology Indore, India (IITI)
- 44 Institut de Physique Nucléaire d'Orsay (IPNO), Université Paris-Sud, CNRS-IN2P3, Orsay, France
- 45 Institut für Informatik, Johann Wolfgang Goethe-Universität Frankfurt, Frankfurt, Germany
- 46 Institut für Kernphysik, Johann Wolfgang Goethe-Universität Frankfurt, Frankfurt, Germany
- 47 Institut für Kernphysik, Technische Universität Darmstadt, Darmstadt, Germany
- 48 Institut für Kernphysik, Westfälische Wilhelms-Universität Münster, Münster, Germany
- 49 Institut Pluridisciplinaire Hubert Curien (IPHC), Université de Strasbourg, CNRS-IN2P3, Strasbourg, France
- 50 Institute for High Energy Physics, Protvino, Russia
- 51 Institute for Nuclear Research, Academy of Sciences, Moscow, Russia
- 52 Institute for Subatomic Physics of Utrecht University, Utrecht, Netherlands
- 53 Institute for Theoretical and Experimental Physics, Moscow, Russia
- 54 Institute of Experimental Physics, Slovak Academy of Sciences, Košice, Slovakia
- 55 Institute of Physics, Academy of Sciences of the Czech Republic, Prague, Czech Republic
- 56 Institute of Physics, Bhubaneswar, India
- 57 Institute of Space Science (ISS), Bucharest, Romania
- 58 Instituto de Ciencias Nucleares, Universidad Nacional Autónoma de México, Mexico City, Mexico
- 59 Instituto de Física, Universidad Nacional Autónoma de México, Mexico City, Mexico
- 60 iThemba LABS, National Research Foundation, Somerset West, South Africa
- 61 Joint Institute for Nuclear Research (JINR), Dubna, Russia
- 62 Korea Institute of Science and Technology Information, Daejeon, South Korea
- 63 KTO Karatay University, Konya, Turkey
- 64 Laboratoire de Physique Corpusculaire (LPC), Clermont Université, Université Blaise Pascal, CNRS-IN2P3, Clermont-Ferrand, France

- 65 Laboratoire de Physique Subatomique et de Cosmologie (LPSC), Université Joseph Fourier, CNRS-IN2P3, Institut Polytechnique de Grenoble, Grenoble, France
- 66 Laboratori Nazionali di Frascati, INFN, Frascati, Italy
- 67 Laboratori Nazionali di Legnaro, INFN, Legnaro, Italy
- 68 Lawrence Berkeley National Laboratory, Berkeley, California, United States
- 69 Lawrence Livermore National Laboratory, Livermore, California, United States
- 70 Moscow Engineering Physics Institute, Moscow, Russia
- 71 National Centre for Nuclear Studies, Warsaw, Poland
- 72 National Institute for Physics and Nuclear Engineering, Bucharest, Romania
- 73 National Institute of Science Education and Research, Bhubaneswar, India
- 74 Niels Bohr Institute, University of Copenhagen, Copenhagen, Denmark
- 75 Nikhef, National Institute for Subatomic Physics, Amsterdam, Netherlands
- 76 Nuclear Physics Group, STFC Daresbury Laboratory, Daresbury, United Kingdom
- 77 Nuclear Physics Institute, Academy of Sciences of the Czech Republic, Řež u Prahy, Czech Republic
- 78 Oak Ridge National Laboratory, Oak Ridge, Tennessee, United States
- 79 Petersburg Nuclear Physics Institute, Gatchina, Russia
- 80 Physics Department, Creighton University, Omaha, Nebraska, United States
- 81 Physics Department, Panjab University, Chandigarh, India
- 82 Physics Department, University of Athens, Athens, Greece
- 83 Physics Department, University of Cape Town, Cape Town, South Africa
- 84 Physics Department, University of Jammu, Jammu, India
- 85 Physics Department, University of Rajasthan, Jaipur, India
- 86 Physikalisches Institut, Ruprecht-Karls-Universität Heidelberg, Heidelberg, Germany
- 87 Politecnico di Torino, Turin, Italy
- 88 Purdue University, West Lafayette, Indiana, United States
- 89 Pusan National University, Pusan, South Korea
- 90 Research Division and ExtreMe Matter Institute EMMI, GSI Helmholtzzentrum für Schwerionenforschung, Darmstadt, Germany
- 91 Rudjer Bošković Institute, Zagreb, Croatia
- 92 Russian Federal Nuclear Center (VNIIEF), Sarov, Russia
- 93 Russian Research Centre Kurchatov Institute, Moscow, Russia
- 94 Saha Institute of Nuclear Physics, Kolkata, India
- 95 School of Physics and Astronomy, University of Birmingham, Birmingham, United Kingdom
- 96 Sección Física, Departamento de Ciencias, Pontificia Universidad Católica del Perú, Lima, Peru
- 97 Sezione INFN, Bari, Italy
- 98 Sezione INFN, Bologna, Italy
- 99 Sezione INFN, Cagliari, Italy
- 100 Sezione INFN, Catania, Italy
- 101 Sezione INFN, Padova, Italy
- 102 Sezione INFN, Rome, Italy
- 103 Sezione INFN, Trieste, Italy
- 104 Sezione INFN, Turin, Italy
- 105 SUBATECH, Ecole des Mines de Nantes, Université de Nantes, CNRS-IN2P3, Nantes, France
- 106 Suranaree University of Technology, Nakhon Ratchasima, Thailand
- 107 Technical University of Split FESB, Split, Croatia
- 108 The Henryk Niewodniczanski Institute of Nuclear Physics, Polish Academy of Sciences, Cracow, Poland
- 109 The University of Texas at Austin, Physics Department, Austin, TX, United States
- 110 Universidad Autónoma de Sinaloa, Culiacán, Mexico
- 111 Universidade de São Paulo (USP), São Paulo, Brazil
- 112 Universidade Estadual de Campinas (UNICAMP), Campinas, Brazil
- 113 University of Houston, Houston, Texas, United States
- 114 University of Jyväskylä, Jyväskylä, Finland
- 115 University of Tennessee, Knoxville, Tennessee, United States
- 116 University of Tokyo, Tokyo, Japan
- 117 University of Tsukuba, Tsukuba, Japan
- 118 Université de Lyon, Université Lyon 1, CNRS/IN2P3, IPN-Lyon, Villeurbanne, France

-
- ¹¹⁹ V. Fock Institute for Physics, St. Petersburg State University, St. Petersburg, Russia
 - ¹²⁰ Variable Energy Cyclotron Centre, Kolkata, India
 - ¹²¹ Vestfold University College, Tonsberg, Norway
 - ¹²² Warsaw University of Technology, Warsaw, Poland
 - ¹²³ Wayne State University, Detroit, Michigan, United States
 - ¹²⁴ Wigner Research Centre for Physics, Hungarian Academy of Sciences, Budapest, Hungary
 - ¹²⁵ Yale University, New Haven, Connecticut, United States
 - ¹²⁶ Yonsei University, Seoul, South Korea
 - ¹²⁷ Zentrum für Technologietransfer und Telekommunikation (ZTT), Fachhochschule Worms, Worms, Germany